TKK Dissertations 208
Espoo 2010

IMAGING STUDIES ON THE FUNCTIONAL ORGANIZATION AND PLASTICITY OF HUMAN VISUAL CORTEX

Doctoral Dissertation

Linda Henriksson

Aalto University
School of Science and Technology
Low Temperature Laboratory

TKK Dissertations 208
Espoo 2010

IMAGING STUDIES ON THE FUNCTIONAL ORGANIZATION AND PLASTICITY OF HUMAN VISUAL CORTEX

Doctoral Dissertation

Linda Henriksson

Dissertation for the degree of Doctor of Science in Technology to be presented with due permission of the Faculty of Information and Natural Sciences for public examination and debate in Auditorium F239a at the Aalto University School of Science and Technology (Espoo, Finland) on the 19th of February, 2010, at 12 noon.

Aalto University
School of Science and Technology
Low Temperature Laboratory

Aalto-yliopisto
Teknillinen korkeakoulu
Kylmälaboratorio

Aalto University
School of Science and Technology
Faculty of Information and Natural Sciences
Department of Biomedical Engineering and Computational Science

Aalto-yliopisto
Teknillinen korkeakoulu
Informaatio- ja luonnontieteiden tiedekunta
Lääketieteellisen tekniikan ja laskennallisen tieteen laitos

Distribution:
Aalto University
School of Science and Technology
Low Temperature Laboratory
Brain Research Unit
P.O. Box 15100
FI - 00076 Aalto
FINLAND
URL: http://ltl.tkk.fi/
Tel. +358-9-470 25619
Fax +358-9-470 22969
E-mail: henriksson@neuro.hut.fi

ISBN 978-952-60-3036-4
ISBN 978-952-60-3037-1 (PDF)
ISSN 1795-2239
ISSN 1795-4584 (PDF)
URL: http://lib.tkk.fi/Diss/2010/isbn9789526030371/

TKK-DISS-2718

Picaset Oy
Helsinki 2010

ABSTRACT OF DOCTORAL DISSERTATION	AALTO UNIVERSITY SCHOOL OF SCIENCE AND TECHNOLOGY P. O. BOX 11000, FI-00076 AALTO, www.aalto.fi

Author Linda Henriksson

Name of the dissertation

Imaging studies on the functional organization and plasticity of human visual cortex

Manuscript submitted 19.10.2009	Manuscript revised 1.2.2010
Date of the defence 19.2.2010	
☐ Monograph	☒ Article dissertation (summary + original articles)

Faculty	Faculty of Information and Natural Sciences
Department	Department of Biomedical Engineering and Computational Science
Field of research	Neuroscience
Opponent	Prof. Martin I. Sereno
Supervisor	Prof. Risto Ilmoniemi
Instructor	Docent Simo Vanni, MD, PhD

Abstract

The visual system occupies approximately 25% of the human cerebral cortex. Large part of the visual cortex is organized into retinotopic maps, in which nearby cortical locations represent neighboring points in the visual field. Based on these retinotopic maps and on functional specialization for particular visual stimuli, such as movement or objects, human visual cortex is divided to more than 20 distinct visual areas. This Thesis contributes to our understanding on the functional organization and reorganization of the human visual cortex.

In the first study, a method for retinotopic mapping based on multifocal functional magnetic resonance imaging (fMRI) responses was developed. Multifocal refers here to parallel stimulation of multiple regions in the visual field using temporally orthogonal stimulus sequences. Multifocal fMRI provides a straightforward analysis and interpretation of the retinotopic responses. The retinotopy in the primary visual cortex (V1), and in a subset of visual areas beyond V1, can be mapped with the multifocal fMRI. In a separate study, the nonlinear spatial summation of the multifocal responses in V1 was characterized. The interactions between adjacent visual field regions suppressed the multifocal responses, most likely due to the far-reaching spatial summation of V1 cells.

The third study showed that training can reorganize visual cortices in an adult patient. The subject was a patient with a chronic visual field defect (homonymous hemianopia) due to a lesion in the visual cortex. We followed the intensive training of visual functions in his blind hemifield with recordings of evoked neuromagnetic responses. After successful training, fMRI measurements revealed an abnormal representation for the trained (right) visual field in the visual areas in the healthy (right) hemisphere, indicating large-scale reorganization of the visual processing.

The fMRI tuning curves for spatial frequency were measured in the fourth study. The spatial frequency evoking the strongest fMRI response decreased with the eccentricity of the visual field. The differences in spatial frequency representation between visual areas support the view that these areas may process visual information at different spatial scales. Finally, the cortical sensitivity to phase relations between different spatial frequencies and the significance of congruent phase structure was revealed in multiple human visual areas. The results suggest that higher-level visual areas use the phase congruency information in the detection of natural broadband edges.

Keywords visual cortex, fMRI, retinotopy, multifocal, plasticity, spatial frequency, phase congruency	
ISBN (printed) 978-952-60-3036-4	ISSN (printed) 1795-2239
ISBN (pdf) 978-952-60-3037-1	ISSN (pdf) 1795-4584
Language English	Number of pages 60 p. + appendices 66 p.
Publisher Aalto University School of Science and Technology	
Print distribution Low Temperature Laboratory, Aalto University School of Science and Technology	
☒ The dissertation can be read at http://lib.tkk.fi/Diss/2010/isbn9789526030371/	

VÄITÖSKIRJAN TIIVISTELMÄ	AALTO-YLIOPISTO TEKNILLINEN KORKEAKOULU PL 11000, 00076 AALTO, http://www.aalto.fi

Tekijä Linda Henriksson

Väitöskirjan nimi

Kuvantamistutkimuksia ihmisen näköaivokuoren toiminnasta ja muovautuvuudesta

Käsikirjoituksen päivämäärä 19.10.2009	Korjatun käsikirjoituksen päivämäärä 1.2.2010
Väitöstilaisuuden ajankohta 19.2.2010	
☐ Monografia	☒ Yhdistelmäväitöskirja (yhteenveto + erillisartikkelit)

Tiedekunta	Informaatio- ja luonnontieteiden tiedekunta
Laitos	Lääketieteellisen tekniikan ja laskennallisen tieteen laitos
Tutkimusala	Neurotiede
Vastaväittäjä(t)	Prof. Martin I. Sereno
Työn valvoja	Prof. Risto Ilmoniemi
Työn ohjaaja	Dosentti Simo Vanni, LT

Tiivistelmä

Ihmisen aivokuoresta noin neljäsosa on omistettu näköaistille. Suuri osa näköaivokuoresta on järjestynyt retinotooppisiksi kartoiksi, joissa vierekkäisillä näkökentän kohdilla on vierekkäiset edustukset aivokuorella. Retinotooppisten karttojen ja toiminnallisten erityispiirteiden kuten liikeherkkyyden perusteella ihmisen näköaivokuori on jaettu yli 20 erilliseen näköalueeseen. Tässä työssä selvitettiin näköalueiden toimintaa ja muovautuvuutta käyttäen toiminnallista magneettikuvausta (fMRI) ja magnetoenkefalografiaa (MEG).

Multifokaalimenetelmällä kartoitetaan samanaikaisesti useiden näkökentän kohtien vasteita käyttäen ortogonaalisia ajoitussekvenssejä. Osatyössä I tätä menetelmää sovellettiin fMRI-vasteisiin perustuvaan retinotooppiseen kartoitukseen. Multifokaalinen fMRI tarjoaa suoraviivaisen tavan mitata ja tulkita retinotooppisia vasteita. Sen avulla retinotopia voidaan kartoittaa ensimmäisellä näköaivokuorella (V1) sekä osalla korkeammista näköalueista. Osatyössä II kartoitettiin multifokaalivasteiden summaation epälineaarisuutta alueella V1. Solujen pitkälle ulottuva spatiaalinen summaatio aiheuttaa todennäköisesti vuorovaikutuksia lähekkäisten näkökentän alueiden edustusten välillä vaimentaen mitattavia multifokaalivasteita.

Osatyössä III osoitettiin, että kuntoutus voi muuttaa aikuisen potilaan näköalueiden toimintaa. Tutkimukseen osallistuneella potilaalla oli näköaivokuoren vaurion seurauksena krooninen näkökenttäpuutos (homonyymi hemianopia). Hän osallistui intensiiviseen kuntoutukseen, jolla pyrittiin parantamaan sokean näkökentän näkökykyä. Kuntoutuksen etenemistä seurattiin herätevastemittauksilla. Menestyksekkään kuntoutuksen jälkeen näkökenttien edustukset kartoitettiin fMRI-mittauksilla. Kuntoutuksen seurauksena sekä sokea (oikea) että normaali (vasen) näkökenttä olivat edustettuina samoilla toiminnallisilla näköalueilla terveellä aivopuoliskolla. Tulokset osoittivat, että kuntoutus voi johtaa suuriin muutoksiin näköalueiden toiminnassa.

Osatyössä IV tutkittiin fMRI-vasteita näköärsykkeen spatiaalitaajuuden funktiona eri kohdissa näkökenttää ja eri näköalueilla. Tulokset tukevat hypoteesia, että varhaiset näköalueet edustavat näkötietoa eri spatiaaliskaaloilla. Osatyössä V tutkittiin vaihesuhteiden käsittelyä näköalueilla. Tulokset viittaavat siihen, että korkeamman tason näköalueet käyttävät spatiaalitaajuuksien välistä vaihekongruenssia tärkeiden piirteiden paikantamiseen.

Asiasanat näköaivokuori, fMRI, retinotopia, multifokaalinen, muovautuvuus, spatiaalitaajuus, vaihekongruenssi

ISBN (painettu) 978-952-60-3036-4	ISSN (painettu) 1795-2239
ISBN (pdf) 978-952-60-3037-1	ISSN (pdf) 1795-4584
Kieli englanti	Sivumäärä 60 s. + liitteet 66 s.

Julkaisija Aalto-yliopiston teknillinen korkeakoulu

Painetun väitöskirjan jakelu Kylmälaboratorio, Aalto-yliopiston teknillinen korkeakoulu

☒ Luettavissa verkossa osoitteessa http://lib.tkk.fi/Diss/2010/isbn9789526030371/

Academic Dissertation

Imaging studies on the functional organization and plasticity of human visual cortex

Author: **Linda Henriksson**
Brain Research Unit, Low Temperature Laboratory
and Advanced Magnetic Imaging Centre
Aalto University School of Science and Technology
Finland

Supervising professor: **Prof. Risto Ilmoniemi**
Department of Biomedical Engineering and
Computational Science
Aalto University School of Science and Technology
Finland

Instructor: **Docent Simo Vanni, MD, PhD**
Brain Research Unit, Low Temperature Laboratory
and Advanced Magnetic Imaging Centre
Aalto University School of Science and Technology
Finland

Preliminary examiners: **Dr. Jozien Goense**
Max Planck Institute for Biological Cybernetics
Department of Physiology of Cognitive Processes
Tübingen, Germany

Docent Teemu Rinne, PhD
Department of Psychology
University of Helsinki
Finland

Opponent: **Prof. Martin I. Sereno**
School of Psychology, Birkbeck College London
and Birkbeck/UCL Centre for NeuroImaging
London, UK;
Department of Cognitive Science
University of California
San Diego, CA, USA

Contents

Preface

This work was carried out in the Brain Research Unit of the Low Temperature Laboratory and in the Advanced Magnetic Imaging Centre at the Helsinki University of Technology (from 1.1.2010 Aalto University School of Science and Technology). I would like to thank the Director of the Low Temperature Laboratory, Prof. Mikko Paalanen, and the Director of the Brain Research Unit, Prof. Riitta Hari, for the excellent working environment.

This Thesis was financially supported by the Finnish Graduate School of Neuroscience (FGSN), Instrumentarium Science Foundation, Finnish Cultural Foundation, Foundation of Technology in Finland and Academy of Finland. Conference and summer school trips were supported by the Magnus Ehrnrooth foundation and the FGSN. I thank all these funding agencies for their crucial support.

I am very grateful to my instructor Docent Simo Vanni for the opportunity to work in his team. I thank him for all the guidance, support and encouragement he has provided to me. Our collaboration with the Visual Science Group and the Neuroinformatics Group from the University of Helsinki through the XtraVision consortium (funded by the Academy of Finland Neuro program) was very important to me. I would like to thank the leaders of these two research groups, Prof. Jussi Saarinen and Prof. Aapo Hyvärinen, for broadening my view of visual neuroscience. I thank Jesper Andersson and Aapo Hyvärinen for being members in my graduate school follow-up group.

I wish to thank my supervising professor, Prof. Risto Ilmoniemi, from the Department of Biomedical Engineering and Computational Science, for his advice and comments during the Thesis writing and examination process. I would also like to thank Prof. (emer) Toivo Katila for his continuous interest in my studies.

I would like to thank all the co-authors of the Publications; Aapo Hyvärinen, Lea Hyvärinen, Andrew James, Lauri Nurminen, Risto Näsänen, Miika Pihlaja, Antti Raninen, and Simo Vanni for the fruitful collaboration. This Thesis was pre-examined by Dr. Jozien Goense from the MPI for Biological Cybernetics, Tübingen, Germany, and Docent Teemu Rinne from the University of Helsinki. I thank them for their insightful comments and suggestions on how to improve the overview part of the Thesis.

I would like to thank all the former and current members and visitors of the Brain Research Unit for the friendly and inspiring atmosphere in the lab. I want to thank the secretaries, especially Pirjo Muukkonen, for taking care of all the administrative paperwork and for helping with the practical issues, and the technical staff for all the support. Special thanks to Marita Kattelus for the assistance with the fMRI measurements, and for the good company.

Many thanks to my wonderful friends and family. My parents have always been very supportive and showed their enthusiasm for research work, thanks! To Matti, I thank you for all the help and encouragement during my studies and research, thanks for being there for me all these years, and thanks for all the love!

Espoo, January 2010

Linda

List of publications

This Thesis consists of an overview and the following five publications:

I. S. Vanni, **L. Henriksson,** and A.C. James. Multifocal fMRI mapping of visual cortical areas. *NeuroImage*, 27(1):95–105, 2005. ©Elsevier Inc.

II. M. Pihlaja, **L. Henriksson**, A.C. James, and S. Vanni. Quantitative multifocal fMRI shows active suppression in human V1. *Human Brain Mapping*, 29(9):1001–1014, 2008. ©Wiley-Liss, Inc.

III. **L. Henriksson**, A. Raninen, R. Näsänen, L. Hyvärinen, and S. Vanni. Training-induced cortical representation of a hemianopic hemifield. *Journal of Neurology, Neurosurgery & Psychiatry*, 78(1):74–81, 2007. ©BMJ Publishing Group Ltd.

IV. **L. Henriksson**, L. Nurminen, A. Hyvärinen, and S. Vanni. Spatial frequency tuning in human retinotopic visual areas. *Journal of Vision (Special issue on Neuroimaging in Vision Science)*, 8(10):5, 1–13, 2008. ©Association for Research in Vision and Ophthalmology.

V. **L. Henriksson**, A. Hyvärinen, and S. Vanni. Representation of cross-frequency spatial phase relationships in human visual cortex. *The Journal of Neuroscience*, 29(45):14342–14351, 2009. ©Society for Neuroscience.

Author's contribution

The author of this Thesis was the principal author in Publications III–V. In Publications IV and V, she designed and performed the main part of the experiments, analyzed the data, and wrote the manuscripts in collaboration with the co-authors. In Publication III, she performed the fMRI experiments, analyzed most of the fMRI and MEG data, and wrote the manuscript with active participation of the co-authors. In Publication I, the author contributed to the planning of the experiments and collecting of the data, analyzed most of the data, developed analysis and visualization tools, and participated in the writing of the manuscript. Publication II was a continuation of Publication I, and the author contributed to the planning of the study and on the writing of the manuscript.

List of abbreviations

BOLD	Blood Oxygenation Level Dependent
CBF	Cerebral Blood Flow
cRF	classical Receptive Field
fMRI	functional Magnetic Resonance Imaging
GLM	General Linear Model
GRE	Gradient-Echo
hV4	human Visual area 4
IPS	Intraparietal Sulcus
LFP	Local Field Potential
LGN	Lateral Geniculate Nucleus
LO	Lateral Occipital area
LOC	Lateral Occipital Complex
MEG	Magnetoencephalography
mffMRI	multifocal functional MRI
MRI	Magnetic Resonance Imaging
MUA	Multi-Unit Activity
NMR	Nuclear Magnetic Resonance
pFus	posterior Fusiform area
PSF	Point Spread Function
rf	radio-frequency
RF	Receptive Field
ROI	Region-Of-Interest
SC	Superior Colliculus
SE	Spin-Echo
SF	Spatial Frequency
SI	Selectivity Index
SPM	Statistical Parametric Map, Statistical Parametric Mapping
TR	Repetition Time
V1	Visual area 1, Primary visual cortex, Striate cortex
V2	Visual area 2, Secondary visual cortex
V3	Visual area 3
V3A	Visual area 3A
V3B	Visual area 3B
V5	Visual area 5
V6	Visual area 6
VEP	Visual Evoked Potential
VP	Ventral Posterior area

1 Introduction

A central goal of visual neuroscience is to understand how the human visual system functions. Humans can rapidly and effortlessly recognize objects in a natural scene, although the appearance of an object varies across different viewpoints and under variations in lighting conditions. No artificial vision system can yet perform the same task as flexibly and accurately. This task is not easy, which is reflected in the amount of brain tissue devoted to vision. In humans, approximately 25% of the cerebral cortex processes primarily visual information (Van Essen, 2004). The visual cortex is divided to tens of distinct visual areas based on studies of lesions that cause selective visual disturbances, on the knowledge of visual processing in animals, and on the functional brain imaging studies. The overall functional organization of the visual cortex continues to be an area of intense research.

This Thesis contributes to the knowledge of visual processing in the low-level visual areas of the human cortex. The specific aims in the functional brain imaging studies of this Thesis are

1. to develop a retinotopic mapping technique based on multifocal stimulation (Publication I),
2. to characterize spatial interactions in the primary visual cortex with the multifocal stimulation technique presented in Publication I (Publication II),
3. to show that the cortical representation of visual field can be reorganized with intensive training of impaired visual functions (Publication III),
4. to compare cortical representations of spatial frequency in different visual areas and visual field locations (Publication IV), and
5. to test cortical sensitivity to cross-frequency phase relations and congruency (Publication V).

This Thesis consists of an overview and five publications (I–V). In this overview, Section 2 introduces the brain imaging methods used in the Publications, and Section 3 gives an introduction to the human visual system. Section 4 summarizes the contribution of the Publications to the knowledge of visual processing in the human visual cortex. Section 5 discusses and draws conclusion on the findings.

2 Structural and functional brain imaging

This Section introduces the brain research methods used in this Thesis. In all Publications (I–V) the main method was functional magnetic resonance imaging (fMRI). Structural MRI provided anatomical reference for the functional results. In addition, magnetoencephalography (MEG) was used in Publication III.

2.1 Magnetic resonance imaging

Magnetic resonance signal

Magnetic resonance imaging (MRI) is based on a physical phenomenon called nuclear magnetic resonance (NMR; Rabi et al., 1938; Bloch et al., 1946; for a general overview of MRI and fMRI, see, *e.g.*, Huettel et al., 2004). MRI of the brain is typically based on the NMR signal from the hydrogen nuclei of the water, because the hydrogen atoms are the most abundant atoms in the human body and the hydrogen nuclei have a high gyromagnetic ratio. Hydrogen nuclei are single protons that have a quantum-mechanical property called spin. In external magnetic field, spins align parallel (low-energy state) or antiparallel (high-energy state) to the magnetic field and precess about the axis of the magnetic field at a characteristic precession frequency known as the Larmor frequency. The Larmor frequency is proportional to the gyromagnetic ratio of the nuclei and to the strength of the magnetic field.

At thermal equilibrium, a small net excess of the spins will align parallel to the external magnetic field creating a net magnetization in the direction of the field. The basic behavior of the net magnetization can be described with classical mechanics, although a detailed description of the NMR phenomenon would require quantum mechanics. The precessing spins can efficiently absorb energy only at the resonance frequency, the Larmor frequency. A radio-frequency (rf) pulse at this frequency will excite the nuclei to transition to the high-energy state. As the populations of the protons in the two energy states are equalized with the rf pulse, the longitudinal component of the net magnetization decreases. The rf pulse also poses phase coherence among the precessing spins and thus introduces a transverse component to the net magnetization. This precessing transverse component is detected as the magnetic resonance (MR) signal.

After the rf pulse, the net magnetization returns to the low-energy equilibrium state and the phase coherence among the precessing protons is gradually

lost. This so-called relaxation of the net magnetization is detected as an exponential decay of the MR signal. Re-growth of the longitudinal component of the net magnetization can be described with time constant T_1 and the decrease of the transverse component with time constant T_2. Inhomogeneities in the magnetic field speed up the transverse relaxation. The transverse relaxation time constant that includes the effects of inhomogeneities in the local magnetic field is called T_2^*.

MR image contrast

In structural brain imaging, image contrast between different tissues is created based on different MR signal strengths. The strength of the MR signal depends on the proton density and on the relaxation time constants. Gray and white matter have different T_1 values and therefore, typical anatomical images of the human brain are so-called T_1-weighted images, in which the white matter appears brighter than the gray matter.

Because the precession frequency depends on the local magnetic field, the spatial location of the MR signal is encoded with gradient magnetic fields that are superimposed on the static external magnetic field. A so-called slice is selected within the total imaging volume by applying a linear magnetic field gradient in one direction and by combining this gradient with the frequency and bandwidth of the rf pulse. Two orthogonal magnetic field gradients encode spatial locations within the slice. The strength of these gradient magnetic fields and the frequency and bandwidth of the rf pulse determine the spatial sampling. The spatial sampling units in MRI are called voxels (volume elements).

The two main imaging parameters that are optimized to enhance a particular image contrast are the time interval between successive rf pulses (repetition time, TR) and the time interval between the rf pulse and the data acquisition (echo time, TE). Before the data acquisition, an echo of the signal is typically created by applying a refocusing pulse or a readout gradient. The combination and timing of different rf pulses, gradients and data acquisition is known as a pulse sequence.

The two most often used pulse sequences are the spin-echo (SE) and gradient-echo (GRE) sequence. The main differences between these two sequences are in the rf pulse and in how they create the echo of the signal. The power and duration of the rf pulse determines the amount of transverse magnetization, and therefore the angle of the net magnetization relative to the external magnetic field, the so-called flip angle. The flip angle in a typi-

cal SE sequence is 90°, whereas in a typical GRE sequence, it is lower than 90°. In a typical SE sequence, the phase coherence between the spins is refocused with a 180° pulse before the data acquisition, whereas in a GRE sequence, the echo of the signal is created with a gradient reversal. The GRE sequence provides faster imaging and stronger MR signal compared to the SE sequence, but the spatial specificity is better with the SE sequence (Yacoub et al., 2003). An entire image can be acquired in a single TR using a technique called echo-planar imaging (EPI). EPI enables fast imaging, which is essential for functional MRI.

2.2 Functional magnetic resonance imaging

Origin of fMRI contrast

The functional MRI data are time-series of images. Functional contrast is created based on changes in the MR signal over time. Most fMRI experiments measure changes in the blood oxygenation level dependent (BOLD) signal (Ogawa et al., 1990, 1992). Oxygenated and deoxygenated blood have different magnetic properties: oxygenated hemoglobin is diamagnetic, whereas deoxygenated hemoglobin is paramagnetic. Deoxygenated hemoglobin increases local inhomogeneity in the surrounding magnetic field and therefore decreases the time constant T_2^*. Thus, typical functional MR images are T_2^*-weighted images, where changes in T_2^* reflect changes in the blood oxygenation.

The BOLD response depends on the oxygen consumption, on the cerebral blood flow (CBF) and on the cerebral blood volume (CBV; for a review see Logothetis, 2008). Oxygen is used for energy production through oxidation of glucose (aerobic metabolism), which is the main energy source for the brain. The brain consumes high amounts of glucose and oxygen even in the "resting state" (for a review, see Raichle and Mintun, 2006). Increased activity in the brain is typically detected as an increased BOLD signal, because an excess amount of oxygenated blood is delivered to the active brain area. The activity-induced increase in the regional CBF and glucose consumption exceeds the increase in the oxygen consumption (Fox et al., 1988).

What does fMRI measure?

Neurons are the cells that transmit and process information in the brain. They transmit rapid electrical signals (action potentials or spikes), communicate with each other via connections called synapses, and are organized

into networks. Our understanding on the neural communication is largely based on invasive electrophysiological studies in animals. BOLD-fMRI results are typically compared with electrophysiological results obtained with single-unit (SUA), multi-unit (MUA) and local field potential (LFP) recordings (for reviews, see Logothetis and Wandell, 2004; Logothetis, 2008). SUA and MUA mostly represent the spiking activity close to the recording site, and thus report the output activity of a single neuron or a small group of neurons. LFP recordings measure low-frequency electrical signals around the recording site, including population synaptic activity, neuromodulatory input and other types of slow signals unrelated to synaptic events. Thus, LFP recordings mainly reflect the input and local processing in a population of neurons rather than the spiking output.

The correlation between the BOLD-fMRI and electrophysiological measurements of neural activity is an active area of research. Concurrent electrophysiological and fMRI measurements in monkeys (Logothetis et al., 2001; Goense and Logothetis, 2008) have demonstrated that the BOLD signal correlates both with the MUA and the LFP responses. LFP has, however, shown to be a more reliable predictor of the BOLD response, because the LFP and BOLD responses remained coupled in situations when MUA decreased but LFP remained unaltered. Thus, it appears that the BOLD response mostly reflects the input and local neural processing in a given neural circuit rather than the output spiking activity (Logothetis, 2008). However, the input and local neural processing typically correlates with the output, and hence the BOLD response typically also correlates strongly with the output spiking activity (Goense and Logothetis, 2008).

Neurovascular coupling

In addition to neurons, another important group of brain cells is the glia. Traditionally, the glial cells have been given a purely supportive role in the nervous system. Recent evidence suggests, however, that the glia actively participate in brain function and also couple the neuronal activity with the regulation of the regional CBF (for reviews, see Haydon and Carmignoto, 2006; Raichle and Mintun, 2006).

Astrocytes are a subpopulation of glia that physically link neurons with the vasculature and have an active role during neural activity (Haydon and Carmignoto, 2006). Active neurons release chemical substances, neurotransmitters, to the space between the neurons (the synaptic cleft). An astrocyte removes the released neurotransmitters from the extracellular space and re-

cycles them back to the neurons creating an increased energy demand in the astrocyte. Astrocytes store glucose in the form of glycogen. Increased anaerobic metabolism of glycogen to lactate can explain the disproportional increase in the glucose uptake and oxygen consumption during functional activation (Shulman et al., 2001). The lactate can be shuttled from the astrocytes to neurons as an energy substrate.

However, it is probably not the increased energy demand that triggers the blood flow response during the neural activity, but instead, the blood flow regulation appears to be directly coupled to the neural activity through the signalling between neurons and astrocytes (Haydon and Carmignoto, 2006). Astrocytes can release a variety of vasoactive agents, *i.e.*, substances that can constrict or dilate the blood vessels. The uptake of the neurotransmitters increases calcium concentration in the astrocyte, which can trigger several vasodilating pathways. Like neurons, the astrocytes are also organized into networks (Giaume et al., 2010), in which a so-called calcium wave can propagate and affect the vasodilation in the local vascular network. The neural activity -dependent calcium signals in the astrocytes may ultimately be the signalling pathway that induces the change in the regional CBF that is coupled to the amount of increased neural activity (Haydon and Carmignoto, 2006).

Spatial and temporal resolution of fMRI

Spatial resolution refers to the ability to distinguish detail in an image. The spatial resolution of an imaging system can be estimated with a point spread function (PSF), which includes all the factors blurring the image. There are several sources for the spatial spreading of the fMRI signal (for reviews, see Logothetis and Wandell, 2004; Logothetis, 2008). These include the coupling between the neural activity and the vasculature, and the spreading of the neural activity along the lateral connections within the cortex. In the human primary visual cortex (V1), the PSF of the fMRI signal is 3–4 mm at field strengths of 1.5–3 T (Engel et al., 1994; Parkes et al., 2005). This spreading is commensurate with the spreading of neural activity along the lateral connections within primate V1 (Grinvald et al., 1994; Angelucci et al., 2002).

The density of the vasculature and the neurovascular regulation of the blood flow also affect the spatial resolution and spatial specificity of the fMRI response. Ideally, the fMRI response would reflect change in the blood flow and oxygenation in the small capillary veins close to the active neural population (Weber et al., 2008). However, larger veins dominate the signals

in typical field strengths of 1.5–3 T. The typical voxel size in an fMRI experiment is (2–4 mm)^3. At this resolution, the main effect of the large veins is that they can displace the activation loci (Olman et al., 2007). At higher field strengths, the signals from smaller vessels and from the capillary bed can be enhanced and the voxel size can be decreased to submillimeter resolution (Goense and Logothetis, 2006; Harel et al., 2006; Yacoub et al., 2008). Altogether, the spatial resolution of fMRI is good compared to other brain imaging method.

The temporal resolution of the fMRI is limited by the neurovascular coupling. The hemodynamic response is sluggish compared to the neural activity and peaks several seconds after the neural activity. Typically, one functional image volume is acquired in 1–3 seconds. With clever experimental design and analysis, however, the neural responses can be studied at subsecond time scale (for a review, see, *e.g.*, Harel et al., 2006).

Experimental design

In a conventional fMRI experiment, relatively long blocks of stimulation alternate with a control condition. To maximize the efficiency of the experiment, each stimulation block typically consists of several repetitions of the same stimulus, and several blocks are measured for each stimulus category. This so-called block design assumes that the fMRI response for the repeated stimuli will remain approximately constant across the repetitions. Block designs are well-suited for experiments in which different stimulus conditions are expected to differ in the magnitude of the fMRI response or to activate spatially non-overlapping brain regions.

The hemodynamic responses for brief or unexpected stimuli can be studied with event-related fMRI. The event-related design is especially useful in experiments, where the stimulus novelty is important or the data is analyzed based on subject's behavioral performance during the experiment. The detection power is weaker in an event-related design than in a block experiment (Liu, 2004); therefore the timing of the stimuli must be carefully optimized in the event-related experiment (Wager and Nichols, 2003).

The functional properties of spatially overlapping neural populations can be studied with an fMRI adaptation design (Grill-Spector et al., 2001). First, the repetition of identical stimuli reduces the fMRI signal. Then, the response is measured for a modified stimulus. The relationship between fMRI adaptation and adaptation of neurons is not fully understood, but the assumption is that if the fMRI signal remains suppressed, the neural population is invari-

ant for the tested modification, and if the fMRI signal recovers, the neural population is sensitive to the tested modification. Adaptation designs were first introduced in visual fMRI studies on invariances in object recognition, but fMRI adaptation has been successfully applied also in studies on neural selectivity in low-level visual processing (*e.g.*, orientation tuning in Fang et al. (2005) and phase sensitivity in Publication V).

Volume-based fMRI data analysis

The fMRI data are first preprocessed to reduce non-task related variability in the data (for a general review, see, *e.g.*, Frackowiak et al., 2003). Each slice within an image volume is acquired at slightly different time point during the data acquisition. These acquisition time differences are corrected with temporal interpolation. Head motion during measurement is corrected with a rigid-body transformation. Head motion can significantly confound the fMRI data, because even after movement correction, some movement-related variance remains in the data. This is mainly because of interactions between head movement and distortions caused by magnetic field inhomogeneity (Andersson et al., 2001). In this Thesis, slice-timing correction and head movement correction were performed for all the fMRI data presented in Publications I–V with SPM2 Matlab toolbox.

The fMRI data are typically analyzed with statistical parametric mapping (SPM; Friston et al., 1994). The time series in each fMRI voxel is modeled with a general linear model (GLM)

$$\mathbf{Y} = \mathbf{X}\beta + \varepsilon, \tag{1}$$

where $\mathbf{Y}$ is a vector that contains the observed responses at a given voxel, $\mathbf{X}$ is a so-called design matrix whose columns represent the expected response, β is a (unknown) parameter vector that contains the coefficients for the columns of the design matrix, and ε is an error or noise vector. The optimal parameters $\hat{\beta}$ that best describe the data can be estimated using a least-squares approach. The design matrix typically includes additional columns for confounding variables in the data. The idea is to remove non-task related variations in the data by modeling confounds such as low-frequency drifts due to movement, physiological noise or MRI scanner instability.

The significance of the estimated parameters $\hat{\beta}$ is tested using statistical tests. With the t statistics, the significance of a particular effect is tested

for each voxel by calculating the t-value $t = c^{\mathrm{T}}\hat{\beta}/\sqrt{\mathrm{Var}(c^{\mathrm{T}}\hat{\beta})}$, where c is a linear contrast. Together the t-values for all the voxels form a statistical parametric map, SPM(t)-map. Because the image volume typically consists of tens of thousands of voxels, testing the significance separately for each voxel increases the possibility of false positives. A correction for this multiple comparison problem can be made using Gaussian random field theory, which takes into account spatial correlations in the statistical map (Friston et al., 1994).

Spatial smoothing of the data improves the validity of the Gaussian random field theory by reducing the effective number of multiple comparisons (Friston et al., 1994). Visual fMRI studies, however, typically omit this preprocessing step, because smoothing decreases the spatial accuracy of the data by spreading the activations across narrow sulci and increasing the partial-volume effects (*i.e.*, averaging across voxels sampling different tissues or functional areas). Omitting the spatial smoothing decreases the validity of the single-voxel statistics, but this can be overcome with functional region-of-interest (fROI) analysis. In the fROI approach, the cortical area of interest is first identified with an independent functional localizer and then a summary measure of the response is calculated from the voxels within that area (Saxe et al., 2006).

Estimates of the magnitudes of the fMRI responses can be calculated from the $\hat{\beta}$ values

$$\%\ \textbf{signal change} = \frac{\hat{\beta}_i^{\mathrm{EOI}}}{\hat{\beta}_i^{\mathrm{mean}}} \cdot 100, \tag{2}$$

where $\hat{\beta}_i^{\mathrm{EOI}}$ is the estimated parameter value (effect of interest) and $\hat{\beta}_i^{\mathrm{mean}}$ is the estimated constant term in voxel i (Publication I). The percent signal change is not an absolute measure of the underlying neural activity. Therefore, it is recommended to compare percent signal changes to various stimuli at a single location or to study spatial maps (*e.g.*, visual field maps) rather than to compare percent signal changes between different locations or different experiments (Logothetis and Wandell, 2004).

Surface-based fMRI data analysis

The human cortex is highly folded, and several brain areas contain a topographic representation that follows this cortical surface and not the volumet-

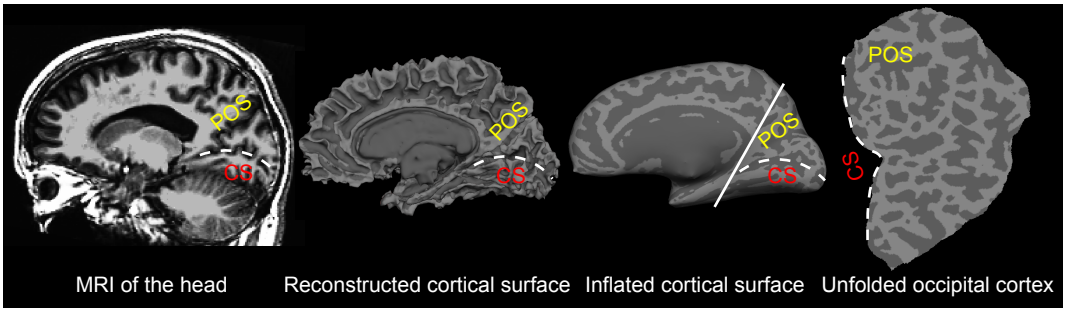

Figure 1: *Cortical surface -based visualization. The cortical surface (calcarine sulcus, CS; parieto-occipital sulcus, POS) is reconstructed based on the boundary between gray and white matter and the reconstruction is inflated and the occipital cortical surface is unfolded with the Freesurfer software (Dale et al., 1999; Fischl et al., 1999a).*

ric coordinate system (Fischl et al., 1999b). In the cortical surface-based analysis (Figure 1), the cortical surface is reconstructed based on the boundary between gray and white matter from an anatomical MRI and the reconstructed surface is either inflated into a smooth three-dimensional surface or unfolded onto a two-dimensional sheet. The visualization of the fMRI result on the cortical surface provides a better view on the spatial extent of the activation and on the spatial relationships between different activation loci.

Group-level analysis of the fMRI data also benefits from the surface-based approach. The size and location of a functional brain area, such as the primary visual cortex, can vary substantially between individuals (Dougherty et al., 2003). Specific brain areas or other regions-of-interest can be defined on the cortical surface separately for each subject. The group-level analysis can be performed on the sets of fMRI responses within the ROIs that represent the same functional area in each subject (Saxe et al., 2006). In addition, the cortical surfaces of different subjects can be aligned based on the sulcal patterns, which improves the intersubject averaging of the functional data (Fischl et al., 1999b).

In this Thesis, surface-based analysis were done either with the Brain à la Carte (BALC) Matlab toolbox (Warnking et al., 2002) or with the Freesurfer software (Dale et al., 1999; Fischl et al., 1999a). With BALC, only part of the occipital cortical surface is reconstructed and unfolded. With Freesurfer, an entire hemisphere is inflated and a part of the cortical surface or the entire hemisphere can be unfolded after making cuts along the three-dimensional surface (Figure 1).

2.3 Magnetoencephalography

Neural basis of MEG signals

With magnetoencephalography (MEG), the weak magnetic field generated by the brain activity is measured from outside of the head (for reviews, see Baillet et al., 2001; Hämäläinen et al., 1993). When a neuron is active, small currents flow in the inside and outside of the cell. These currents generate a magnetic field, but because the neural currents are extremely weak, simultaneous activity of tens of thousands of parallel cells is required for a measurable external magnetic field.

A neuron consists of a cell body, an axon and dendrites. The branching dendrites and the cell body receive signals from other neurons via synapses. At the synapse, the presynaptic neuron releases the neurotransmitters, which modulate ion fluxes through the membrane of the postsynaptic neuron. The ion flows induce an electrical potential difference between the synaptic location and the cell body. The potential difference causes a current to flow inside the cell (the so-called primary current). A current flowing in the opposite direction in the outside of the cell closes the electrical circuit (the so-called volume current). These currents flowing in the inside and outside of the cell generate the magnetic field.

The two main groups of neurons in the cortex are the stellate and pyramidal neurons. The pyramidal neurons are the main source for the magnetic fields measured with MEG, because these cells have large dendritic trunks, which are aligned approximately parallel to each other and perpendicular to the cortical surface. Thus, the synchronous activation of a pyramidal cell population can generate a magnetic field that can be measured from the outside of the head.

MEG measurements

Very sensitive sensors are needed to detect the weak biomagnetic signals. Typically an array of SQUIDs (superconducting quantum interference devices) is used, and the measurements are done in a magnetically shielded room. To reduce noise, event-related MEG responses are typically averaged across multiple stimulus presentations.

MEG can follow the dynamics of brain activity on a time scale of milliseconds. Thus, the temporal resolution of MEG is superior to fMRI. On the other hand, the spatial resolving power of MEG is typically much worse

than that of fMRI, because the source currents evoking the measured external magnetic fields cannot be uniquely defined from the MEG data. Source modeling aims to estimate the source configuration that best matches the measured MEG signals.

In this Thesis, MEG was used in Publication III to follow changes in cortical activity during training. The advantages of MEG over fMRI in a follow-up study include the direct coupling between neural activity and the measured response, and the high reproducibility of the responses.

3 The human visual system

This Section gives an introduction to the human visual system with an emphasis on the functional organization of the human visual cortex.

3.1 Pathway from the eye to the brain

Retina

Information processing in the human visual system begins in the retinal photoreceptor cells at the back of the eyes (Figure 2). The human retina contains two types of photoreceptors: cones and rods. Rods are responsible for vision in low light (scotopic vision, "night vision") and cones for vision in daylight (photopic vision). The density of cones is the highest in the central retina, an area called fovea, where visual acuity is the best. The density of cones and the visual acuity drops rapidly towards the peripheral retina (Curcio et al., 1990).

The photoreceptors convert light into electrical signals, whereafter a multilayered circuit of retinal interneurons and ganglion cells contribute to the processing of visual information (for a review, see Field and Chichilnisky, 2007). Retinal ganglion cells are the output cells that convey information from the retina to the brain. The receptive field (RF) of a visual cell is the region of visual field where a stimulus alters the cell's firing rate. A retinal ganglion cell typically has a concentric center–surround receptive field (Figure 3A). The retinal ganglion cell increases its firing rate, when a spot of light hits the center of the RF, but not the surround. A ganglion cell can also have the opposite RF organization, in which case a dark spot in the center and light in the surround maximally excites the cell.

Natural visual input is highly correlated (neighboring points or pixels in an image have similar values). It has been suggested that the center–surround RF organization acts to decorrelate the retinal code (Atick and Redlich, 1992). In addition, retinal ganglion cells adjust their sensitivity to the mean intensity of the input (light adaptation), which enables the cells to function over the huge range of normal daylight intensities (Laughlin, 1989). The cells adapt also to the range of light intensities (contrast adaptation), which enable the cells to use their dynamic range efficiently (Smirnakis et al., 1997).

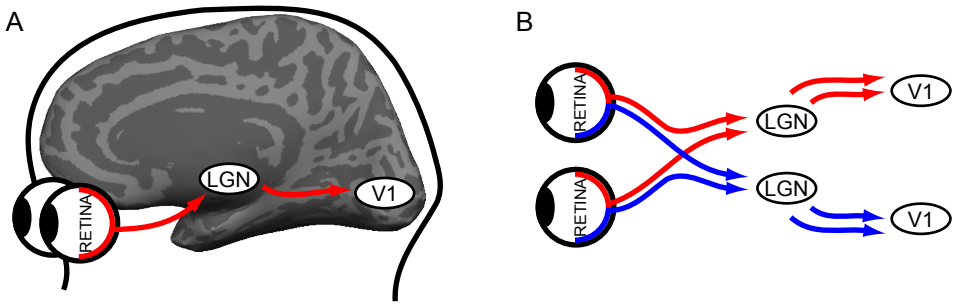

Figure 2: *Pathway from the eye to the visual cortex. A) The main pathway from the retina of the eye to the primary visual cortex (V1) passes through the lateral geniculate nucleus (LGN) of the thalamus. B) The axons of the retinal ganglion cells, which are the output cells from the retina, partially cross at the optic chiasm. Thus, the left visual hemifield is represented in the right hemisphere and the right hemifield in the left hemisphere.*

From the retina to the visual cortex

Lateral geniculate nucleus (LGN) of the thalamus is the main link between the retina and the visual cortex (Figure 2). At least three parallel (magno-, parvo- and koniocellular) pathways transfer segregated information about the retinal image (for a review, see Lennie and Movshon, 2005). The magnocellular pathway projects to the cortex via the magnocellular layers of the LGN and carries information about the spatial and temporal characteristics of the retinal image. The parvocellular and koniocellular pathways convey color information. The red-green opponency and spatial details are carried by the parvocellular pathway, which projects through the parvocellular layers of the LGN to the cortex. The koniocellular pathway convey the blue-yellow opponent signals (Hendry and Reid, 2000).

The receptive fields of LGN cells have the concentric center–surround organization (Figure 3A), similar to the RF structure of the retinal ganglion cells. Because the function of the LGN cells appear to mirror the function of the retinal ganglion cells, LGN has been traditionally considered as a passive relay between the retina and cortex. However, LGN receives extensive feedback from the cortex, and recent studies suggest that LGN has an important role in regulating the information flow to the cortex (for a review, see Saalmann and Kastner, 2009).

The primary visual cortex (V1) is probably the most intensively studied

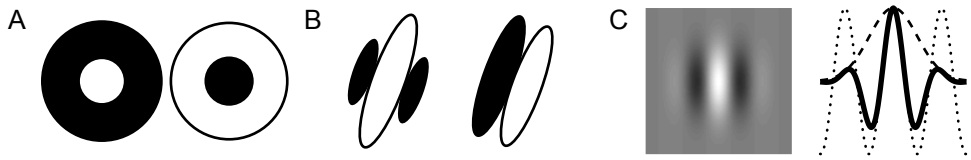

Figure 3: *Receptive fields in the retina, LGN and primary visual cortex. A) In the retina and LGN, cells typically have concentric center–surround receptive fields. On the white region (in the center or surround), light increases cell's firing rate, and on the black region, darkness increases the firing rate. B) In V1, cells have oriented receptive field. C) The receptive field of a V1 simple cell can be modelled with a Gabor filter (cross-section shown with solid black line), which is a multiplication of a sinusoidal (dotted line) with a Gaussian envelope (dashed line).*

region of the brain. The majority of our knowledge about the function of V1 has been gathered in electrophysiological recordings on cats and monkeys. The macaque monkey is the primary animal model for human visual system, because the anatomies and psychophysical performances are comparable.

3.2 Primary visual cortex

Receptive fields

In the classic papers, Hubel and Wiesel (1962; 1968) studied the receptive fields of V1 cells in cats and monkeys. They classified the cells as simple or complex based on responses to simple visual stimuli such as light spots and bars. A simple cell had an RF that resembled an orientation-specific edge or line detector (Figure 3B). The cell increased its firing rate, when a light bar of the correct orientation and width was presented in its receptive field. Complex cells had more complex receptive fields and were described to derive from convergent input from simple cells.

Movshon *et al.* (1978) reported that simple cells show spatial summation of inputs across the receptive field. Therefore, a spatiotemporal filter provides a more comprehensive description of the simple cell RF than an edge detector. The characteristic sensitivities of a simple cell RF can be captured with a Gabor filter (Figure 3C), which is a multiplication of a sinusoidal function with a Gaussian envelope (Jones and Palmer, 1987; Ringach, 2002). The Gabor filter model captures the location and size of the RF and its sensitivity to the orientation and spatial frequency of the input. Simple cell gives

a strong response when a patch of grating with the parameters it is most sensitive to (also called preferred or optimal) is presented to its RF.

Complex cells in V1 are also sensitive to the orientation and spatial frequency of the input but are less sensitive to the position of the stimulus (or the phase of a grating stimulus) than simple cells. Therefore, the complex cell RF is often modeled with a quadrature pair of simple cell RFs (Carandini et al., 2005). Recent studies estimating the RFs using reverse correlation methods suggest that an even better description of the complex cell RF is obtained with several additional filters (Rust et al., 2005; Chen et al., 2007).

Spatial summation and center–surround interactions

The size and location of a cell's receptive field can be mapped by moving a small stimulus across the visual field and by defining the RF as the region, which increases the cell's firing rate. This measure of the RF size is commonly referred to as the classical RF (cRF) or the minimum response field, because the cell's response can be modulated by stimuli far outside this region (for reviews, see Fitzpatrick, 2000; Lennie and Movshon, 2005).

In natural visual environment, the stimulus falling into a cell's RF is typically part of a larger context. The surrounding context can suppress or facilitate the cell's response to its optimal stimulus centered at the cRF (Fitzpatrick, 2000; Lennie and Movshon, 2005). Typically, the cell's response is most effectively suppressed by a surrounding stimulus whose parameters match the preferences of the cRF, and the response can even be enhanced by a surrounding stimulus whose parameters mismatch the optimal stimulus.

The extent of the RF can also be defined as the area over which an expanding stimulus elicits an increasing response and refer to it as the cell's summation field (Cavanaugh et al., 2002a; Angelucci et al., 2002). Summation fields can be several times larger than the cRFs, because they include regions that modulate the cells response only when presented simultaneously with a stimulus at the cRF. If the size of the stimulus is increased beyond the summation field, the cell's response typically decreases before reaching an asymptote (note, however, that cells do not behave identically, see Cavanaugh et al., 2002a). The modulatory surround field can be defined based on the smallest stimulus at which the response asymptotes. Comparing the extents of summation fields and cortical connections, Angelucci *et al.* (2002) and Cavanaugh *et al.* (2002a) concluded that horizontal connections within V1 create the summation field and feedback signals from higher visual areas create the modulatory surround field.

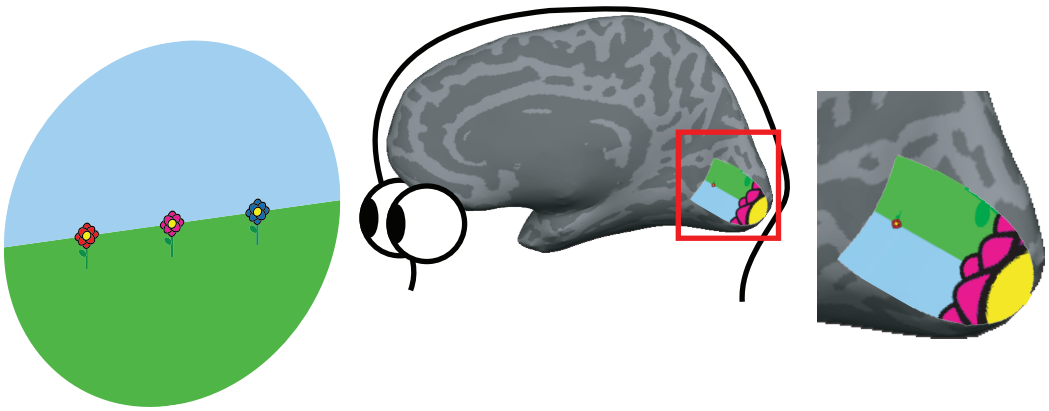

Figure 4: *Representation of visual field in the primary visual cortex. The left visual hemifield is represented on the occipital lobe of the right hemisphere. The center of the visual field (fovea) is represented on the occipital pole. The cortical representation is inverted and the representation of the fovea is greatly expanded. The two-dimensional visual field was mapped to the two-dimensional cortical surface using a mathematical model of the V1 topography (Schwartz, 1980; Polimeni et al., 2006).*

Retinotopic organization and cortical magnification

The receptive field centers create an orderly representation of the visual field: neighboring cells respond to neighboring locations in the visual field. This topographic representation is called a retinotopic map or a visual field map. The cortical area devoted to the central visual field (fovea) is much larger than the area devoted to an equal sized region in the peripheral visual field (Figure 4). Correspondingly, the average size of the receptive field increases as function of the visual field eccentricity (Van Essen et al., 1984; Dumoulin and Wandell, 2008).

The expanded representation of the central visual field can be described with cortical magnification, typically expressed as millimeters of cortical surface per degree of visual angle (Daniel and Whitteridge, 1961). The cortical magnification has been carefully quantified in monkey V1 using electrophysiology (Daniel and Whitteridge, 1961; Tootell et al., 1982) and radioactive labelling (Tootell et al., 1982). The first estimates of cortical magnification in human visual cortex were based on correlations between visual field deficits and locations of cortical lesions (Holmes, 1918; Horton and Hoyt, 1991b). fMRI has enabled more accurate estimates of the cortical magnifi-

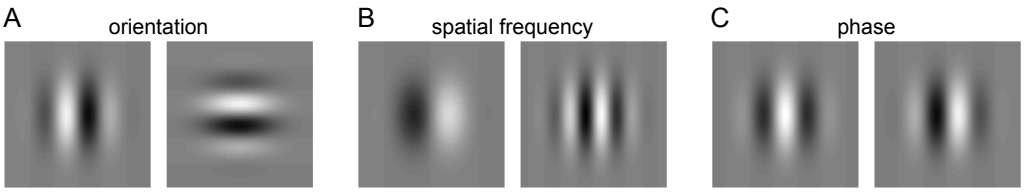

Figure 5: *Receptive fields of V1 simple cells. Simple cells differ, for example, in the A) orientation, B) spatial frequency, and C) phase preferences.*

cation within human V1 based on representation of the central (Engel et al., 1994; Sereno et al., 1995; Duncan and Boynton, 2003) and peripheral visual field (Stenbacka and Vanni, 2007).

Representation of orientation and spatial frequency

Each position in the visual field is analyzed by several cells that have overlapping RF locations but different sensitivities to other stimulus dimensions (Hubel and Wiesel, 1968; De Valois et al., 1982), such as orientation or spatial frequency (Figure 5). Electrophysiological and optical imaging studies have characterized the distributions of these parameters in populations of V1 cells.

The cortex is organized vertically into so-called cortical columns, in which cells in different cortical layers are connected and share a similar response property (for a review, see Mountcastle, 1997). The cortical columns related to different response properties are mapped within the cortex at different spatial scales. In the ocular dominance columns, the cells respond to a stimulus either in the left or the right eye. In the orientation columns (Hubel and Wiesel, 1968), the cells respond best to a particular orientation. Tangentially along the cortex, cells in the adjacent cortical columns vary systematically in the ocularity and orientation selectivity. Cells in neighboring columns have similar orientation preferences, which creates a smoothly varying cortical representation of orientation on the cortical surface.

The cortical representation of spatial frequency (SF) is less clear than that for the orientation, but optical imaging studies suggest that similar SF preferences cluster and form a smoothly varying representation of SF on the cortical surface (Issa et al., 2000). Thus, populations of V1 cells tile the visual space and jointly represent the orientations and SFs.

Computational studies have tried to explain the observed distribution of RFs in V1. A popular approach has been to explore correlations between regularities in natural images and neural processing (for reviews, see Simoncelli and Olshausen, 2001; Hyvärinen et al., 2009). The idea is that the RFs in V1 are optimized during evolution and individual development to represent natural input efficiently. Computational models based on statistics of natural images have succeeded in deriving families of V1-like RFs from the statistical properties of natural images (Olshausen and Field, 1996; Hyvärinen and Hoyer, 2000), which suggests that the V1 RFs form an efficient representation of natural visual input.

3.3 Functional organization of human visual cortex

Identification of visual areas

In humans, approximately 25% of the cerebral cortex is devoted to vision (Van Essen, 2004). Human visual cortex (Figure 6) is divided to more than 20 visual areas (for reviews, see Wandell et al., 2007; Grill-Spector and Malach, 2004). The total number of reported visual areas keeps growing with the improvements in imaging techniques and stimulus paradigms (Arcaro et al., 2009; Silver and Kastner, 2009). In animal studies, visual areas have been traditionally defined by four independent criteria: cytoarchitecture (arrangement of cells within the tissue), connections with other cortical and subcortical structures, retinotopic organization, and functional properties. The last two criteria have been applied to human fMRI data.

Visual areas V1, V2 and V3 have clear retinotopic organizations and these areas can be identified based on the distinct retinotopic maps. In monkeys, at later stages of the visual processing, the retinotopic organization becomes more coarse and visual areas become selective to increasingly complex stimuli (Kobatake and Tanaka, 1994). Selective activation by complex stimuli, such as motion or objects, can be used to localize these areas in humans. The idea of functional specialization for specific stimulus attributes in distinct cortical areas originally stems from selective visual disturbances after damage to localized regions in the cortex.

Retinotopy and functional specialization

Areas V1, V2 and V3 are often called early or low-level visual areas, because activity in these areas correlates with processing of local, low-level visual features and with the perception of local image elements (Grill-Spector and

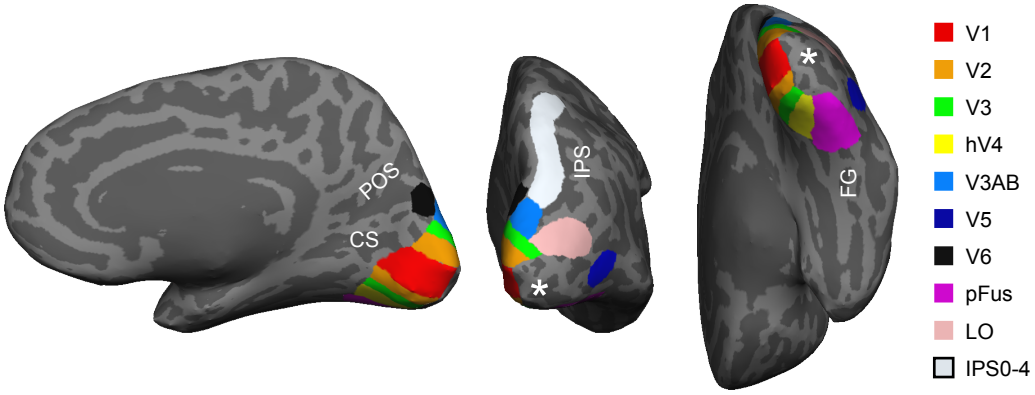

Figure 6: *A subset of visual areas in the human cortex. The medial, posterior and ventral views of the right hemisphere (CS = calcarine sulcus; POS = parieto-occipital sulcus; IPS = intraparietal sulcus; FG = fusiform gyrus) show the approximate locations of visual areas V1, V2, V3, V3AB, hV4, V5, V6, pFus (posterior fusiform area), LO (lateral occipital area) and IPS0–4 (areas around intraparietal sulcus). The asterisk (*) denotes the location of the central (foveal) visual field representation at the occipital pole (the foveal confluence), where it is more difficult to resolve the borders between visual areas.*

Malach, 2004). These areas are typically identified in the human visual cortex based on the retinotopic organizations (see Section 4.2). Almost all visual input passes through the primary visual cortex before reaching the higher-level areas. Therefore, V1 is essential for normal visual function. Area V1 represents the contralateral visual hemifield (Figure 4) and a lesion in V1 causes an almost complete loss of visual functions of the corresponding region in the visual field of both eyes (Holmes, 1918; see, however, Section 4.3). Areas V2 and V3 presumably also contribute to local visual processing and somehow integrate the output from V1, but their exact role in visual processing is still unclear (Boynton and Hegde, 2004). Both areas are split into two parts (Figure 6), each representing a quadrant of the contralateral visual field. The ventral V3 can also be referred to as VP (ventral posterior area). A lesion confined in V2/V3 produces up to a quadrantic visual field defect limited to the horizontal meridian (Horton and Hoyt, 1991a).

Damage to the ventral occipital cortex can impair perception of color (achromatopsia; for a review, see Zeki, 1990), but the relationship between color processing and individual visual areas has been controversial. Functional MRI studies have indicated sensitivity to color in the human ventral

occipital cortex (McKeefry and Zeki, 1997; Hadjikhani et al., 1998; Brewer et al., 2005; Wade et al., 2008). A visual area named human V4 (hV4) responds to color stimuli in the same way as the monkey V4 (Wade et al., 2008), but the retinotopic organizations in monkey and human V4 differ substantially (Brewer et al., 2005; Wade et al., 2008). In contrast to the quadrant visual field representations in the macaque dorsal and ventral V4, hV4 most likely represents the full contralateral visual hemifield (Brewer et al., 2005; Wandell et al., 2007; Wade et al., 2008). Adjacent to hV4, an area named V8 (Hadjikhani et al., 1998) has also been identified based on a distinct visual field representation and high responsiveness to color, but its relation to area hV4 is unclear.

Areas V3A, V5 and V6 show sensitivity to dynamic visual stimuli. Area V3A is retinotopically organized and is more sensitivity for visual motion than areas V1, V2 and V3 (Tootell et al., 1997). Based on retinotopic data, an area named V3B has been recently identified adjacent to area V3A (Wandell et al., 2007). Area V5 (also called MT or hMT) is essential for motion perception. Low-level visual areas do respond to moving stimuli, but V5 is necessary for global motion processing (Grill-Spector and Malach, 2004). A bilateral lesion around this area causes motion blindness (akinetopsia; Zihl et al., 1983, for a review, see Zeki, 1991) and neuroimaging studies indicate high selectivity for moving stimuli in V5 (Tootell et al., 1995). When area V5 is localized based on its selectivity for visual motion, the localized functional region typically includes also adjacent motion-sensitive areas (*e.g.*, area MST) that can be identified based on detailed retinotopic analysis (Huk et al., 2002). Thus, this area is commonly referred to as V5+ or MT+ complex. Area V6 has been recently identified in humans using wide-field fMRI retinotopic mapping (Pitzalis et al., 2006; Stenbacka and Vanni, 2007). Area V6 shows selectivity for coherent motion of random dot fields and the retinotopic organization has a relative emphasis on the peripheral visual field (Pitzalis et al., 2010, 2006).

The lateral occipital complex (LOC) shows a stronger response when the subject views images of objects than images with scrambled structure. The LOC can be divided to a dorsal area termed the lateral occipital (LO) area (Malach et al., 1995) and a ventral region located around the posterior fusiform gyrus (pFus; Grill-Spector et al., 1999). Object representations in these areas show invariances to visual cues (*e.g.*, line drawings vs. motion contours) and spatial transformations (*e.g.*, size and position) and the activity is correlated with object perception (Grill-Spector and Malach, 2004). Based on retinotopic responses, the lateral and ventral occipital cortices can

be further divided to several distinct visual areas (Brewer et al., 2005; Larsson and Heeger, 2006; Arcaro et al., 2009).

Areas selective to specific object categories (*e.g.*, faces, places, tools) have been reported in the human visual cortex (Grill-Spector and Malach, 2004). For example, an area around the fusiform gyrus (FFA, fusiform face area; Kanwisher et al., 1997) shows replicable face-selective responses and a lesion around this area impairs the recognition of familiar faces. Therefore, it could be that distinct cortical areas represent specific object categories. An alternative hypothesis is that object representations are distributed and overlapping within the object-selective areas (Haxby et al., 2001).

Multiple visual areas along the intraparietal sulcus (IPS) have been recently identified based on distinct visual field representations (Swisher et al., 2007; Saygin and Sereno, 2008). These areas are typically not activated with a simple checkerboard stimulus, but require that the subject actively attends to the stimulus (Saygin and Sereno, 2008). With a retinotopic stimulus combined with a task that captures attention to the stimulus, several retinotopic areas have been identified in the parietal and frontal cortex (Saygin and Sereno, 2008; Silver and Kastner, 2009). Because the functional specializations within these areas is mainly unknown, the areas in the parietal cortex are commonly named as IPS0/1/2/3/4 according to the anatomical locations. IPS0 likely corresponds to the area previously named as V7 (Tootell et al., 1998). Eye movements (saccades), attention and visuomotor control of movements activate these areas strongly (Astafiev et al., 2003), but object-selective responses have also been reported (Konen and Kastner, 2008).

Ventral and dorsal streams

Two main hypothesis about the organization of the visual cortex are hierarchical processing (Felleman and Van Essen, 1991; Barone et al., 2000) and parallel processing streams (for a review, see Ungerleider and Haxby, 1994). The hierarchical organization was originally based on detailed descriptions of the anatomical connections between visual areas in monkeys. Based on the feedforward and feedback connections between visual areas and on the lateral connections within visual areas, Felleman and Van Essen (1991) suggested that visual information is processed along a sequence of cortical areas with progressively larger and more complicated receptive fields.

Visual areas can be divided into two main parallel processing streams: dorsal and ventral streams (Figure 7). The dorsal stream is associated with spatial or motion vision and the ventral stream with object recogni-

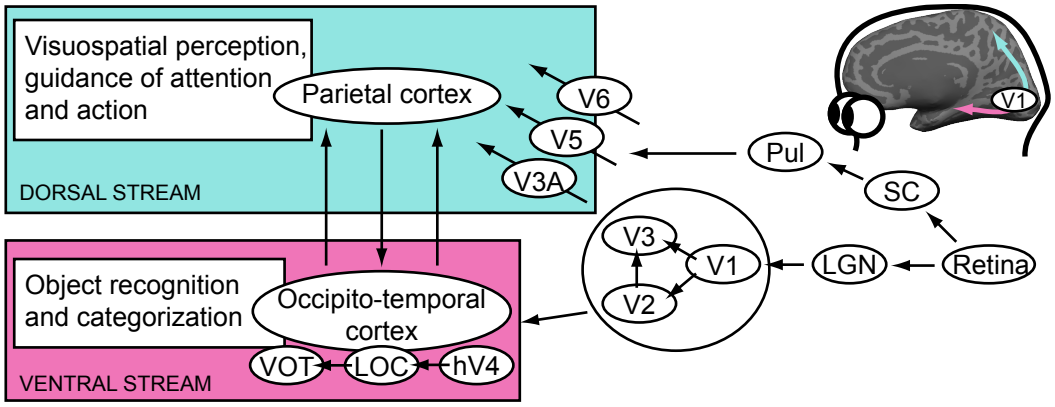

Figure 7: *The dorsal and ventral streams. Visual areas can be divided into two processing stream: ventral stream for object recognition (Ungerleider and Haxby, 1994) or vision-for-perception (Goodale and Milner, 1992) and dorsal stream for spatial vision (Ungerleider and Haxby, 1994) or vision-for-action (Goodale and Milner, 1992). Visual areas within and between processing streams show various forms of interactions, e.g., the extensive feedback connections from higher-level to low-level (V1, V2 and V3; circled in the figure) areas are not shown here for the sake of simplicity (figure adapted from Orban, 2008).*

tion (Ungerleider and Haxby, 1994). Early fMRI data supported the view that spatial localization is restricted to the dorsal stream (Malach et al., 1995), but recent studies have shown retinotopic organization in the vicinity of the object-selective areas in the lateral occipital cortex (Larsson and Heeger, 2006; Sayres and Grill-Spector, 2008). Ventral stream areas appear to carry information both on the category of an object and on its location in the visual field (Schwarzlose et al., 2008; Sayres and Grill-Spector, 2008).

The ventral pathway can also be called as the ”perceptual” stream and the dorsal stream as the ”action” stream, because lesions in the dorsal stream can affect the use of vision for guidance of actions (optic ataxia; impairs, *e.g.*, accurate grasping), whereas lesions in the ventral stream can cause impairments in the perception or recognition of objects (Goodale and Milner, 1992). The overall functional organization of the visual cortex continues to be an area of intense research.

4 Studies on functional organization of human visual cortex

4.1 Experimental setup

The fMRI experiments were performed on a General Electric 3 T scanner equipped with an eight-channel phased-array or a single-channel quadrature head coil in the Advanced Magnetic Imaging Centre at Helsinki University of Technology. The BOLD-fMRI data were acquired using the gradient-echo echo-planar imaging sequence. Details of the data acquisition are given in the Publications. The MEG measurements were performed using a whole-head 306-channel Vectorview (Elekta Neuromag Oy) neuromagnetometer in the Low Temperature Laboratory at Helsinki University of Technology. The visual stimuli were created with Matlab (MathWorks, Inc.). The stimulus timing was synchronized with the MR image acquisitions and controlled with the Presentation software (Neurobehavioral Systems, Inc.). The stimuli were displayed on a semitransparent screen via a data projector.

The subjects were healthy adults with normal or corrected-to-normal vision, except in Publication III, where the subject was an adult patient with a chronic visual field defect. In Publications I–III the subjects passively fixated a point in the middle of the screen while the stimuli were presented at some distance from this fixation point. In Publications IV and V the subjects performed a task in the fixation point to direct attention away from the stimuli. Eye movements were not recorded; However, in Publications I and II, the fact that we could map the retinotopic responses with the multifocal stimulus implies that the subjects maintained good fixation. In Publication III, we carefully controlled stable fixation with control measurements (for details, see the publication). In Publications IV and V, the subjects' good performance in the fixation task implies that they maintained good fixation.

4.2 Visual field representation with multifocal fMRI (Publications I and II)

Measuring visual field maps with fMRI

The first studies on visual field maps in human visual cortex were based on correlations between visual field deficits and locations of cortical lesions (Holmes, 1918; Horton and Hoyt, 1991b). Nowadays, a standard method to map the retinotopic organization is to use a periodic visual stimulus moving

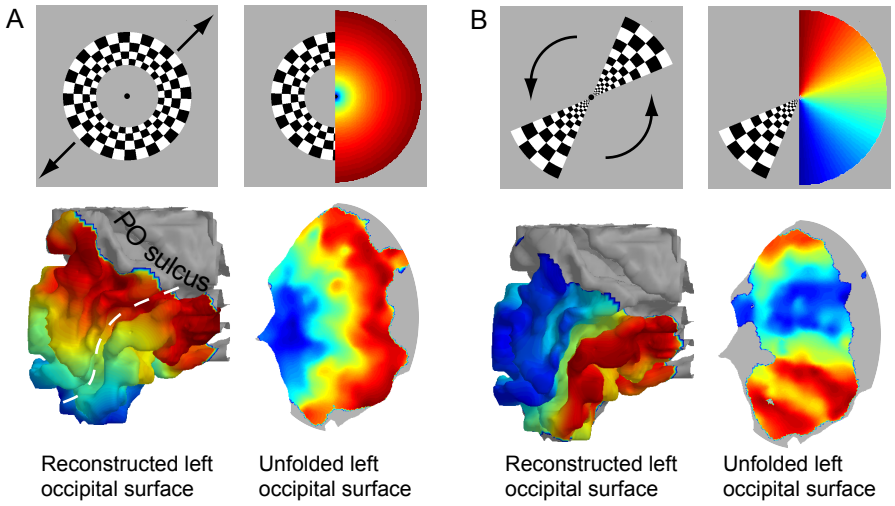

Figure 8: *Phase-encoded retinotopic mapping of human visual cortex. A) fMRI responses to expanding and contracting ring stimuli map the cortical representation of the visual field eccentricity and B) responses to rotating wedge-shaped stimuli map the cortical representation of the polar angle. A) Representative visual field eccentricity map (calcarine sulcus is marked with a white dashed line) and B) visual polar angle map were analyzed with Brain à la Carte (BALC) Matlab toolbox for the analysis of phase-encoded retinotopic data (Warnking et al., 2002).*

across the visual field and to decode the visual field representation from the phase of the travelling waves of fMRI activity (Engel et al., 1994).

The visual field eccentricity (distance from fovea) is typically mapped with an expanding and contracting ring stimulus and the polar angle (meridional position) with a clockwise and counterclockwise rotating wedge-shaped stimulus (Figure 8). Visual field is represented multiple times in the human cortex and the borders between visual areas can be outlined from the alternation of the visual field representation between mirror and non-mirror representations (Sereno et al., 1995).

Multifocal mapping of retinotopic organization (Publication I)

Publication I presents a multifocal (mf) stimulation method to measure visual field maps in the human visual cortex. Multifocal refers to parallel stimulation of several visual field locations with temporally orthogonal stimulus sequences. Multifocal methods are widely used in the topographic mapping

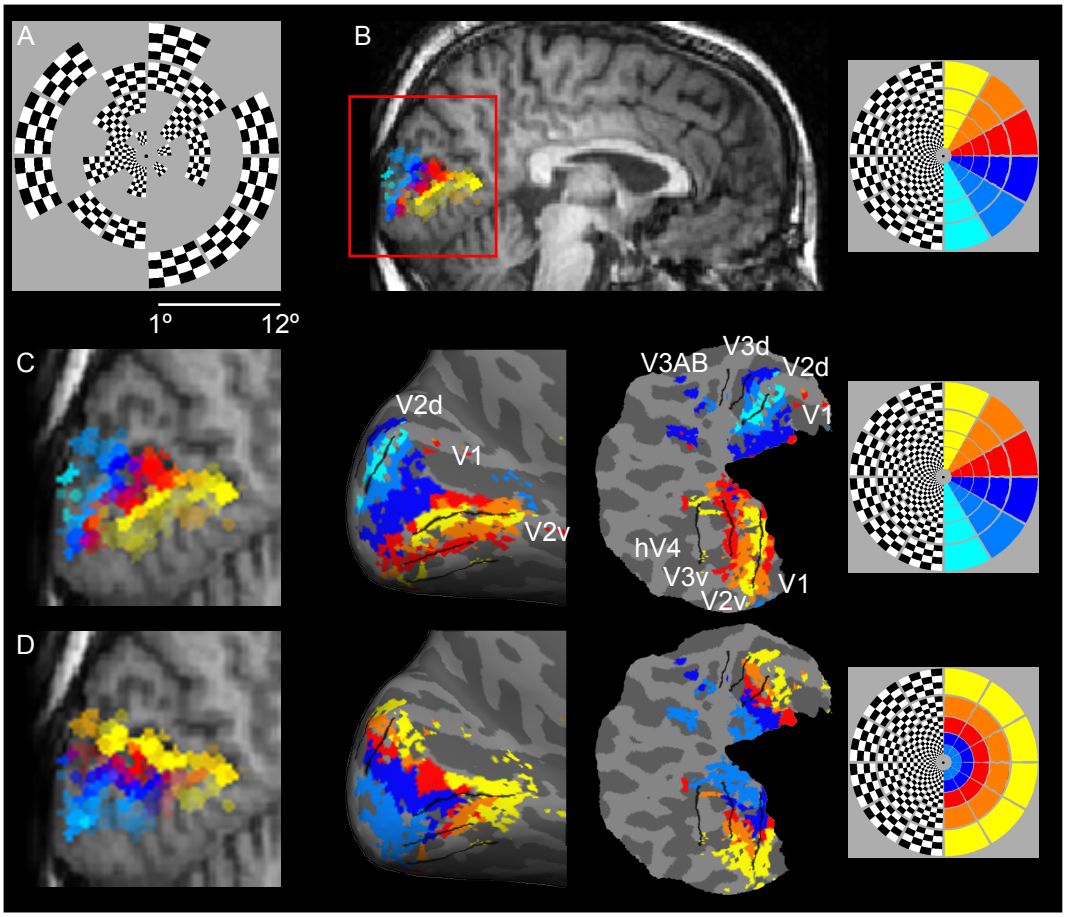

Figure 9: *Multifocal retinotopic mapping in human visual cortex with a 60-region stimulus (Publication I). A) Visual field from 1° to 12° is divided into 60 regions with stimulated regions scaled according to the cortical magnification. Each region changes from active (checkerboard pattern stimulation) to inactive (mean luminance) based on a temporally orthogonal stimulation sequence. B) The fMRI activation clusters for the 30 stimulus regions in the right hemifield are color-coded based on the polar angle of the stimulated regions to illustrate the visual field polar angle map (single-subject data). The primary visual cortex in the occipital cortex around the calcarine sulcus contains a complete representation of the contralateral visual hemifield. C) The polar angle map is visualized over the subject's MRI image (same as in B), on the subject's reconstructed cortical surface and on the unfolded cortical surface. Black lines indicate the boundaries between visual areas. For this subject, the activation clusters are mainly confined to visual areas V1 and V2. D) In the visual field eccentricity map the fMRI activation clusters are color-coded based on the eccentricity of the stimulated regions. The visual field eccentricity map is visualized over the subject's MRI image and on the reconstructed cortical surface.*

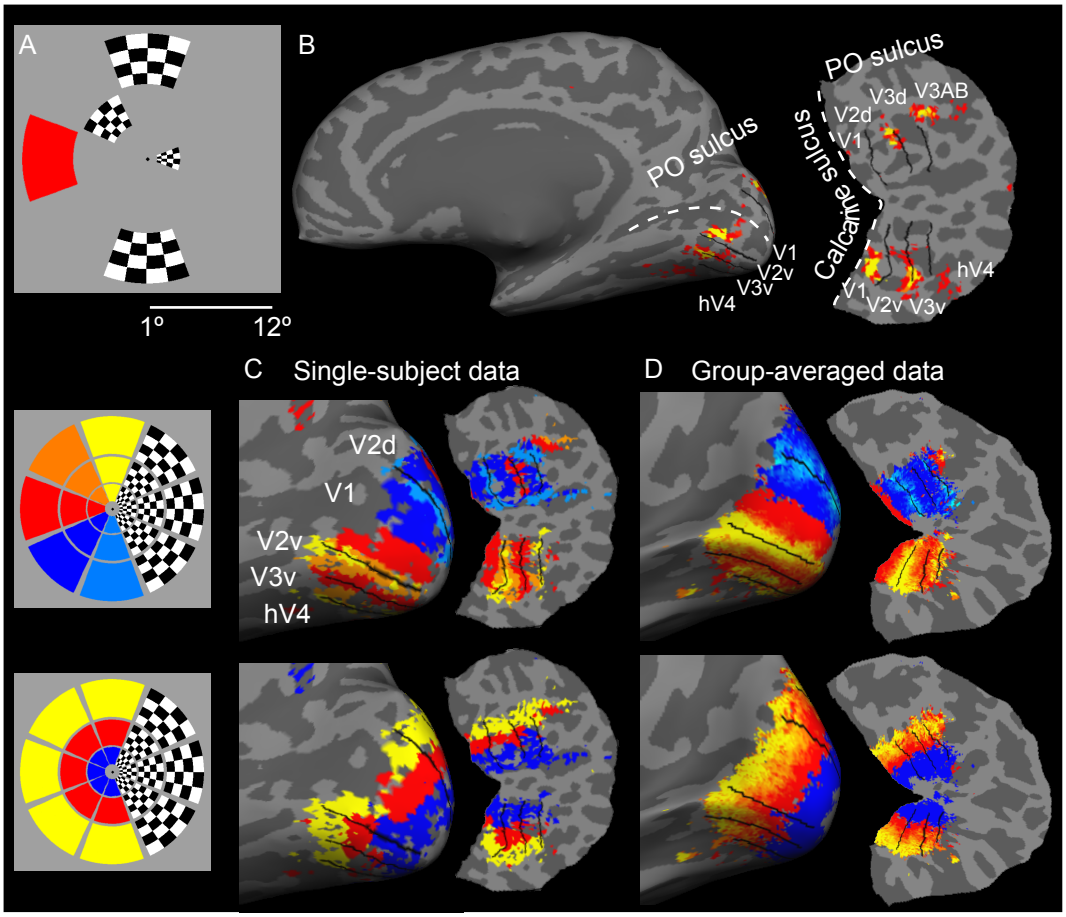

Figure 10: *Multifocal retinotopic mapping of human visual cortex with a 24-region multifocal stimulus. A) One frame of the 24-region multifocal stimulus. The stimulus regions are scaled according to the cortical magnification. Neighboring regions in the stimulus were presented in two different temporal windows to enhance cortical responses. B) Activation pattern for one stimulus region in the 24-region multifocal stimulus (red region in A) is shown on a subject's reconstructed and inflated cortex. Black lines indicate the boundaries between visual areas. The stimulus region was over the left horizontal meridian and correspondingly activated visual areas V1, V2, V3, hV4 and V3AB in the right hemisphere. C) The activation clusters create a visual field map on the cortical surface when color-coded according to the visual field polar angle (upper row) or eccentricity (lower row). Note the retinotopic responses in visual areas V3, hV4 and V3AB. The 24-region stimulus gives more reliable retinotopic responses in the extrastriate cortex across subjects than the 60-region stimulus (Figure 9). D) Visual field eccentricity and polar angle maps averaged across ten subjects in the spherical surface-based coordinate system implemented in the Freesurfer software (Fischl et al., 1999b).*

of retinal responses (multifocal electroretinography, for a review, see Hood, 2000) and visual evoked potentials (multifocal VEPs, Baseler et al., 1994).

In most previous mf studies, the timing of the stimulation is based on a maximal length binary sequence (m-sequence) and the analysis of the data relies on cross-correlation between the stimulation sequence and the response. James (2003) introduced a more flexible orthogonal sequence to multifocal stimuli and, instead of cross-correlation, analyzed VEP responses using a general linear model (GLM) approach. Publication I applied the mf stimulation sequence and the GLM approach from James (2003) to fMRI.

In Publication I, the visual field from 1° to 12° eccentricity was divided to 60 regions (Figure 9A). The timing of stimulation in each region followed a temporally orthogonal sequence, so-called quadratic residue sequence

$$t = \sum_{j=0}^{N-1} j^2 \mathrm{mod} N, \tag{3}$$

where N is a prime, which defines the length of the sequence. In our stimulation sequence, N is the smallest prime above the number of stimulus regions and of the form $4K-1$, where K is an integer (for example, with 60 stimulus regions N equals 67). Equation 3 gives the timing of stimulation for one stimulus region. For each subsequent region (i), the temporal sequence given by Equation 3 is cyclically delayed

$$t_i = (t_{i-1} - k) \mathrm{mod} N, \tag{4}$$

where k is a prime.

The responses for the multifocal stimuli were analyzed with the GLM approach implemented in SPM2 Matlab toolbox for fMRI data analysis. In V1, each region in the multifocal stimulus evoked a spatially localized fMRI response. Figure 9 illustrates how the local multifocal responses reveal the visual field map both in the volume- and surface-based visualizations.

Beyond V1, only a subset of the 60 regions evoked statistically significant response (Figure 9C–D). The signal-to-noise ratio of the multifocal responses in the extrastriate visual areas can be enhanced with modified stimulus parameters. Figure 10 shows that the multiple visual field maps can be localized

with a 24-region multifocal stimulus. Next section discusses a possible explanation for the enhancement of the extrastriate responses with a reduced number of stimulus regions.

Center–surround interactions suppress multifocal responses (Publication II)

In the analysis of the multifocal data (Publication I), we assumed independent fMRI responses for each of the 60 stimulus regions and linear spatial summation of the responses. Electrophysiological studies have shown, however, that V1 cells show nonlinear spatial summation. The response of a cell to a stimulus placed at the receptive field can be suppressed by a stimulus presented to the surround (for a review, see Fitzpatrick, 2000). This response suppression between multiple adjacent visual stimuli has also been demonstrated in human V1 using fMRI (Kastner et al., 2001; Zenger-Landolt and Heeger, 2003). In Publication II, we characterized the spatial interactions in the multifocal fMRI data.

The spatial interactions within human V1 were examined by comparing responses to spatially and temporally identical stimuli (Figure 11A) presented either alone (unifocal condition) or as part of a 9-region multifocal stimulus (multifocal condition). Figure 11B shows that the mean fMRI signal from the same region-of-interest (ROI) was significantly reduced in the multifocal condition compared to the unifocal condition. That is, the surrounding regions in the multifocal design significantly suppressed the response of the central region.

The origin of the suppression in the multifocal condition was further assessed using modified stimuli. Reducing the contrast of the stimuli reduced the responses, but preserved the suppression (Figure 11C). Modifying the orientation or spatial frequency of the surrounding regions relative to the center reduced the suppression (Figure 12). These results indicate a neural origin for the suppression, because the surround suppression in single cells is also the strongest when the stimulus attributes of the center and surround are matched (Cavanaugh et al., 2002b).

We examined the spreading of activation on the cortical surface from the unifocal condition. Cortical distances between the midpoints of stimulated regions were calculated using the estimate of cortical magnification in human V1 (Duncan and Boynton, 2003). The spreading was stronger in the ROIs representing the surrounding regions that shared a border with the central region in the multifocal stimulus (mean center-to-center distance between

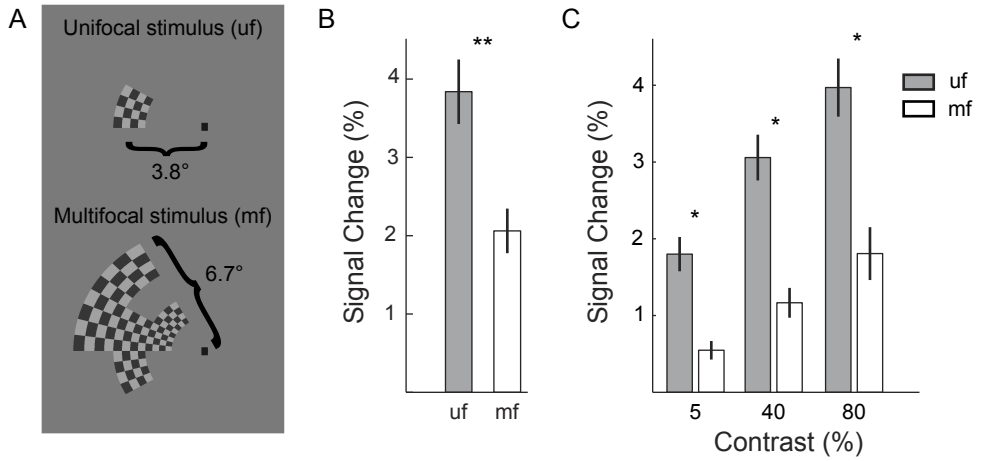

Figure 11: *Center–surround suppression and multifocal responses in V1 (Publication II). A) Example frames of the unifocal (uf, 1-region) and multifocal (mf, 9-region) stimuli. The spatial and temporal properties of the stimulation sequences were identical for the uf stimulus and for the central region in the multifocal stimulus. B) Mean fMRI responses from V1 for the uf stimulus and for the central region of the mf stimulus averaged across nine subjects (**$p < 0.01$). C) Mean fMRI responses from V1 for the uf stimulus and for the central region of the mf stimulus at different contrasts averaged across eight subjects (*$p < 0.05$).*

cortical representations: ca. 6 mm) than for the ROIs representing the regions sharing only a corner with the central region (mean center-to-center distance between cortical representations: ca. 9 mm). The spreading was minimal when the distance between the midpoints of the stimulus regions increased to 9 mm on the cortical surface. The spreading was also affected by the contrast of the stimulus. The extent of the spreading of the cortical activation to the neighboring cortical locations is commensurate with the extent of far-reaching horizontal connections within primate V1 (Angelucci et al., 2002). The horizontal connections, which have been suggested to mediate interactions within the spatial summation fields of macaque V1 cells (Angelucci et al., 2002), could therefore mediate also the interactions between representations of adjacent regions in the multifocal stimulus.

As a conclusion, the center–surround interactions significantly suppress the multifocal responses already in V1 (Figure 11). In the higher-level visual areas, the extent of the suppressive interaction scale with the receptive field size (Kastner et al., 2001). Therefore, the nonlinear interactions between

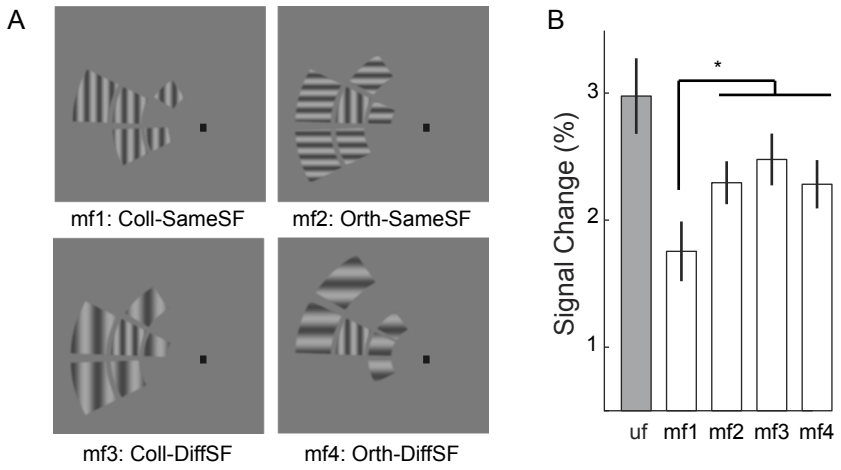

Figure 12: *Modulation of the center–surround interactions and multifocal responses in V1 (Publication II). A) Example frames of four different multifocal (mf, 9-region) stimuli. The unifocal stimulus and the central region were always identical (grating stimulus with fixed orientation and spatial frequency). B) Mean fMRI responses from V1 for the uf stimulus and for the central region of the four different mf stimuli averaged across eight subjects. Suppression of the response from the central region is the strongest when the surrounding regions share the same orientation and same spatial frequency (mf1) with the central region (*$p < 0.05$).*

spatially adjacent stimulus regions likely affect the magnitude of multifocal responses even more beyond V1. These far-reaching interactions most likely explain, why we failed to map the retinotopic maps in the extrastriate areas with the 60-region mf stimulus (Figure 9), but succeeded in this task with the 24-region stimulus (Figure 10). In the 24-region stimulus, in addition to increasing the size and decreasing the number of stimulus regions, the neighboring regions in the stimulus were presented in two different temporal windows to enhance the cortical responses.

4.3 Training-induced reorganization of visual field representation in adult brain (Publication III)

Neural plasticity in adult brain

Neural plasticity is the remarkable ability of the brain to adapt and reorganize with experience and by interacting with the environment. Plasticity in

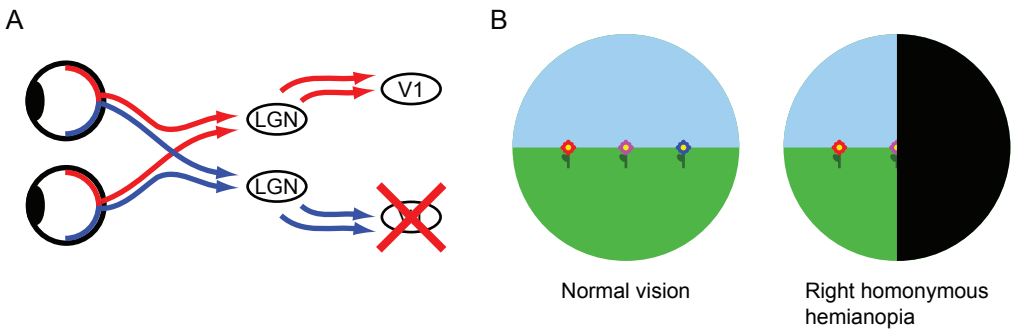

Figure 13: *Homonymous hemianopia. A) A complete lesion of the primary visual cortex causes B) blindness of the contralateral (opposite) visual hemifield in both eyes.*

the cortex is most evident during development, but changes in the cortical representations are also possible in adulthood. Large-scale reorganizations of somatosensory (Merzenich et al., 1984; Pons et al., 1991) and motor cortices (Nudo and Milliken, 1996) are well documented in animal studies. In humans, recovery from a stroke requires cortical reorganization to compensate for the lost motor, sensory and language functions (for a review, see Rossini et al., 2003). In addition to the spontaneous recovery, rehabilitation of movement induces functional reorganization in the primary motor cortex, which is associated with a significant clinical improvement (Liepert et al., 2000).

The reorganization of the adult visual system has been under controversy. Plasticity in the primary visual cortex after retinal dysfunction has been described both in adult animals (Gilbert and Wiesel, 1992; Kaas et al., 1990) and humans (Baker et al., 2005), but the negative results (Smirnakis et al., 2005; Sunness et al., 2004) have created a confusion about the capacity of adult V1 for major long-term reorganization.

Cortical blindness and training of impaired visual functions

A lesion in the primary visual cortex causes blindness in the corresponding regions of the visual field. Homonymous hemianopia (Figure 13), cortical blindness of a visual hemifield in both eyes, is relatively common in elderly population (Gilhotra et al., 2002). Instead of total blindness, the affected hemifield may have residual sensitivity to visual stimuli (for a review, see Stoerig and Cowey, 1997). This residual vision in the blind hemifield can be conscious visual sensations or unconscious blindsight. A blindsighted patient can make above-chance guesses about the parameters (*e.g.*, position or

direction of movement) of a visual stimulus presented in the blind hemifield.

Residual vision has been associated with subcortical pathways that bypass the lesioned V1 and project directly to extrastriate areas (Figure 16A). Stimulation of the affected hemifield typically activates dorsal extrastriate visual areas, especially the motion sensitive area V5 (Ptito et al., 1999; Baseler et al., 1999). Similarly, in monkeys a lesion in area V1 preserves residual visual sensitivity in the affected hemifield and neural responsiveness in the dorsal stream areas (for a review, see Bullier et al., 1994).

Rehabilitation of vision in hemianopic patients is not a standard clinical procedure, albeit both compensatory (Kerkhoff et al., 1992; Nelles et al., 2001) and restorative (Zihl and von Cramon, 1979; Kasten et al., 1998; Zihl, 2000; Julkunen et al., 2003; Sabel et al., 2004) training approaches have provided promising results. Training of eye movements improves visual search within the affected hemifield and hence compensates for the visual field defect (Kerkhoff et al., 1992; Nelles et al., 2001). Visual restitution training aims at enlargements in the actual functional visual field, but the positive results (Zihl and von Cramon, 1979; Zihl, 2000; Kasten et al., 1998) have conflicted with claims of uncontrolled eye movements (Balliet et al., 1985; Pommerenke and Markowitsch, 1989; Horton, 2005). Vision restoration therapy, VRT, is also a trademark of NovaVision, Inc. (Boca Raton, FL, USA).

In typical VRT, the border zone between the intact and impaired visual fields is trained with daily practise of light detection. The size of the visual field is typically measured by detecting small static or slowly moving stimuli in multiple locations. The results depend critically on the stimulus characteristics (Sabel et al., 2004). Because the residual vision is most sensitive to large, high-contrast, moving or flickering stimuli, the typical clinical visual field test may be beyond the abilities of a damaged visual system.

An alternative training approach is to train the visual sensitivity deep within the blind hemifield (Hyvärinen et al., 2002; Sahraie et al., 2006; Raninen et al., 2007; Huxlin et al., 2009). The detection and recognition sensitivity within the blind hemifield can be restored without enlargements of the functional visual field as defined with the standard clinical perimetry (Hyvärinen et al., 2002; Raninen et al., 2007) and the improvements can be transferred to other tasks (Huxlin et al., 2009). Recently, the effect of VRT was also improved when the small light stimuli within the border zone were replaced with larger stimuli within the blind hemifield (Jobke et al., 2009).

Training-induced neural plasticity in adult visual cortex (Publication III)

Publication III shows in an adult chronic homonymous hemianopia patient that successful training of vision can be associated with cortical reorganization of the visual field representation. In this case study, the patient was a 61 years old male who had right homonymous hemianopia due to a stroke. In the chronic stage (22 months after the stroke), he began intensive training of the residual vision in the blind hemifield. The training included difficult detection tasks of flickering discs and recognition of flickering letters. In general, a difficult task is required for plastic changes to take place in the cortex (Blake et al., 2006). After five months of training, the sensitivity in the blind hemifield was comparable to the sensitivity in the normal hemifield (for details on the training and psychophysical results, see Raninen et al., 2007).

The effect of the training was followed with magnetoencephalography. Figure 14A shows the evoked responses for a stimulus in the blind (right) hemifield for all follow-up MEG measurements. The first significant response emerged approximately three months after the training, and after 13 months of training, the response amplitude increased remarkably (for details on the follow-up MEG results, see Raninen et al., 2007). Figure 14B illustrates the change in the MEG field patterns. Importantly, the MEG responses for the blind (right) field stimulation appeared to the ipsilateral (right) hemisphere, to the same hemisphere with the normal hemifield responses.

After the successful training, the cortical reorganization was mapped with fMRI. Figure 15 shows the fMRI activation patterns for a stimulus either in the trained (right) or normal (left) hemifield. In accordance with the MEG results, the trained hemifield is represented in the ipsilateral (right) hemisphere. The surface-oriented analysis in Figure 15B shows that both hemifields are represented in the same set of cortical areas in the intact hemisphere. Such extensive ipsilateral representation is not seen in healthy individuals (Tootell et al., 1998).

Publication III, together with the accompanying paper by Raninen et al. (2007), demonstrates that training of impaired visual functions can lead to major reorganization of the adult visual cortex. What anatomical pathway could mediate the ipsilateral representation of the trained visual field (Figure 16)? Residual vision in hemianopic patients is typically assumed to be mediated by a subcortical pathway that bypasses V1 in the lesioned hemi-

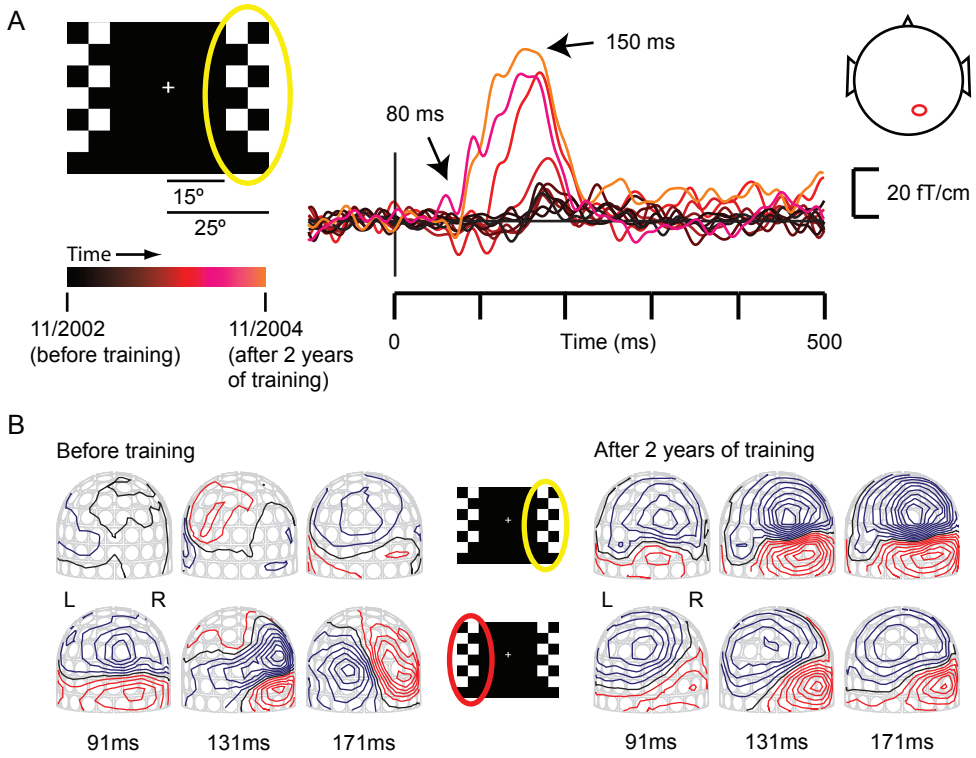

Figure 14: *Training-induced changes in MEG responses for a hemianopic patient. A) The evoked responses are shown for a checkerboard stimulus in the right (hemianopic) hemifield for all follow-up measurements (modified from Raninen et al., 2007). The red ellipse on the schematic head shows the location of the MEG sensor. The color codes the measurement date. During the training, the evoked responses emerged over the right hemisphere. B) The magnetic field patterns are shown for the pattern-reversals of the checkerboard stimulus in the right/hemianopic (upper panel) or left/normal (lower panel) hemifield before (left panel) and after (right panel) the training (Publication III). The contrast-reversals in the hemifields occurred in a random order. The MEG helmet is viewed from the back. Before the training, the stimulus in the right (hemianopic) hemifield evoked no measurable response. After 2 years of training, stimulus in either hemifield evoked a strong response over the right hemisphere.*

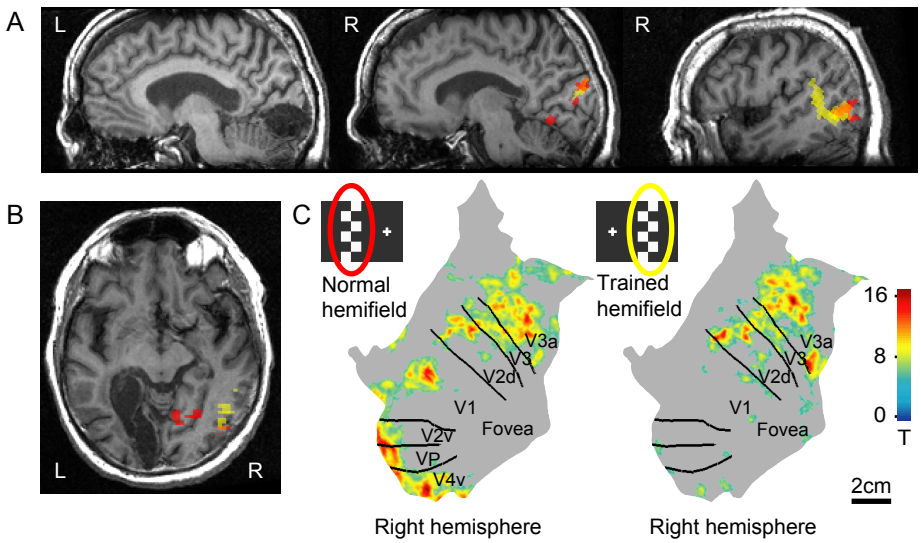

Figure 15: *Training-induced cortical reorganization of visual field representation (Publication III). A–B) The lesion covered medial parts of the left occipital cortex, including V1. Consistent with the MEG results (Figure 14), the fMRI activations were on the right occipital cortex regardless of the hemifield stimulated (red = left/normal hemifield, yellow = right/trained hemifield, L = left, R = right). C) The same fMRI activations as in A and B are shown on the patient's reconstructed and unfolded cortical surface of the right hemisphere. The trained visual hemifield is represented in the same set of cortical areas with the normal hemifield.*

sphere (Ptito et al., 1999). Recent diffusion tensor imaging (DTI) studies on humans confirm such anatomical connections between superior colliculus, pulvinar and cortex (Leh et al., 2008; Lanyon et al., 2009) and directly between LGN and V5 (Bridge et al., 2008). Interhemispheric connections between V5 could distribute the activity between hemispheres (Bridge et al., 2008; Leh et al., 2008). Such a pathway is, however, an improbable explanation for the MEG and fMRI responses for the "blind" field stimulation in our case (Figure 15), because the stimuli evoked only marginal activity in the lesioned hemisphere, and because the MEG data showed an early peak of activity in the ipsilateral (intact) hemisphere (Figure 14). For the same reasons, interhemispheric connections between V1 (Hagmann et al., 2007) appear an improbable explanation, although this is the pathway suggested to mediate ipsilateral fMRI activation in early visual areas in healthy subjects (Tootell et al., 1998).

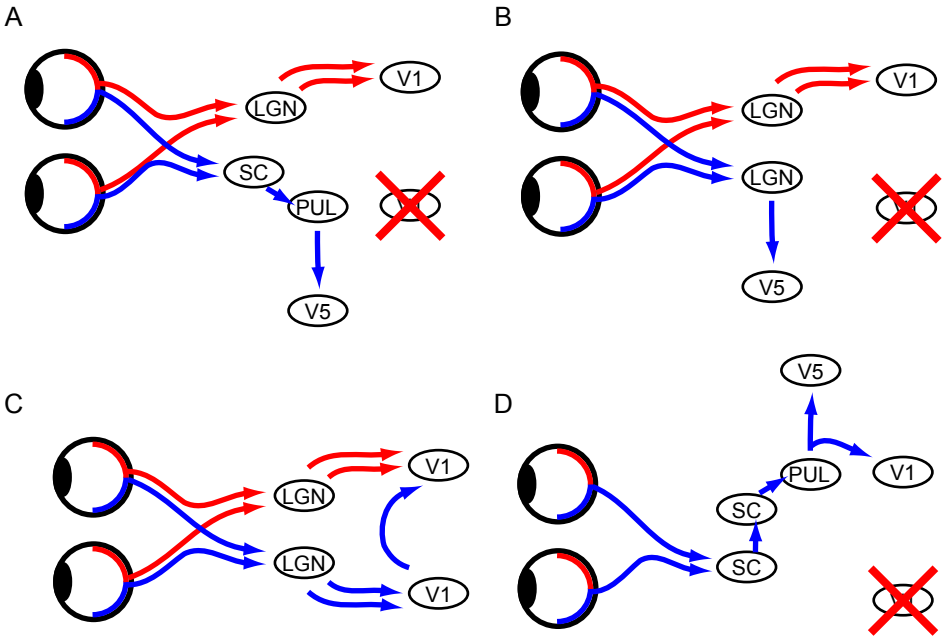

Figure 16: *Possible pathways mediating residual, ipsilateral and trained vision. A) In addition to LGN, superior colliculus (SC) receives retinotopically organized input from the retina and connects to the cortex via pulvinar. This is the subcortical pathway that has been suggested to mediate residual vision in hemianopia patients (Ptito et al., 1999; Leh et al., 2008). B) LGN also connects directly to extrastriate area V5 (Bridge et al., 2008). C) Interhemispheric connections between V1 (Hagmann et al., 2007) can explain ipsilateral fMRI activations in healthy subjects (Tootell et al., 1998). D) Interhemispheric connections between superior colliculus appear essential for blindsight in hemispherectomized patients (Leh et al., 2006). This pathway including connections of the superior colliculus between the hemispheres, and pulvinar and visual cortex in the intact hemisphere could explain the ipsilateral representation of the trained hemifield (Figure 15).*

Our suggestion is that the ipsilateral responses (Figures 14 and 15) are conveyed via a strengthened subcortical pathway that includes callosal connections of the superior colliculus (SC) between the hemispheres, and pulvinar and visual cortex in the intact hemisphere (Figure 16D). This is the pathway that most likely mediates blindsight in hemispherectomized patients Bittar et al., 1999; Leh et al., 2006). Hemispherectomy is a surgical treatment for severe epilepsy in which an entire hemisphere is removed or disconnected. Hemispherectomized patients with blindsight have strong ipsilateral

and contralateral projections from the SC to the visual areas in the remaining hemisphere, whereas hemispherectomized patients without blindsight show no such connections (Leh et al., 2006).

4.4 Representation of spatial frequency in human visual cortex (Publication IV)

Spatial frequency selectivity of cortical cells

Selectivity for spatial frequency (SF) is one of the prominent properties of cells in the primary visual cortex. A tuning function is typically used to describe a cell's response to different SFs. Cells in the macaque V1 typically have quite narrow SF tuning functions (De Valois et al., 1982), *i.e.*, they respond only to a limited range of SFs around the peak SF. Different cells within the same cortical location respond to different ranges of SFs, and therefore each position in the visual field is analyzed by several simple cells that have overlapping RF locations but different SF sensitivities (De Valois et al., 1982).

The representation of spatial frequency is not uniform across macaque V1, but the mean SF preference decreases with increasing visual field eccentricity (Schiller et al., 1976; De Valois et al., 1982). At similar eccentricity, the mean SF preference is lower in macaque area V2 than in area V1 (Foster et al., 1985) and in area V3 lower than in area V2 (Gegenfurtner et al., 1997). Beyond V1, the function of early visual areas is still poorly understood. The differences in SF tuning together with a recent study on complex shape selectivity (Hegde and Van Essen, 2007) suggest, however, that the processing in the early visual areas might be quite similar, but could take place at different spatial scales.

Spatial frequency tuning in human visual cortex (Publication IV)

Publication IV examined how the neural SF tuning shows up in the fMRI responses. Measuring fMRI tuning curves may provide an important link between electrophysiological single-cell studies and fMRI studies. This study focused on differences in SF tuning at different visual field eccentricities and visual areas in humans.

The stimuli were drifting angular sinusoidal gratings modulated with Gaussian envelopes both in angular and radial directions (Figure 17A,C). Angular gratings were selected instead of cartesian gratings, because these stimuli allow the presentation of a large range of SFs into the periphery

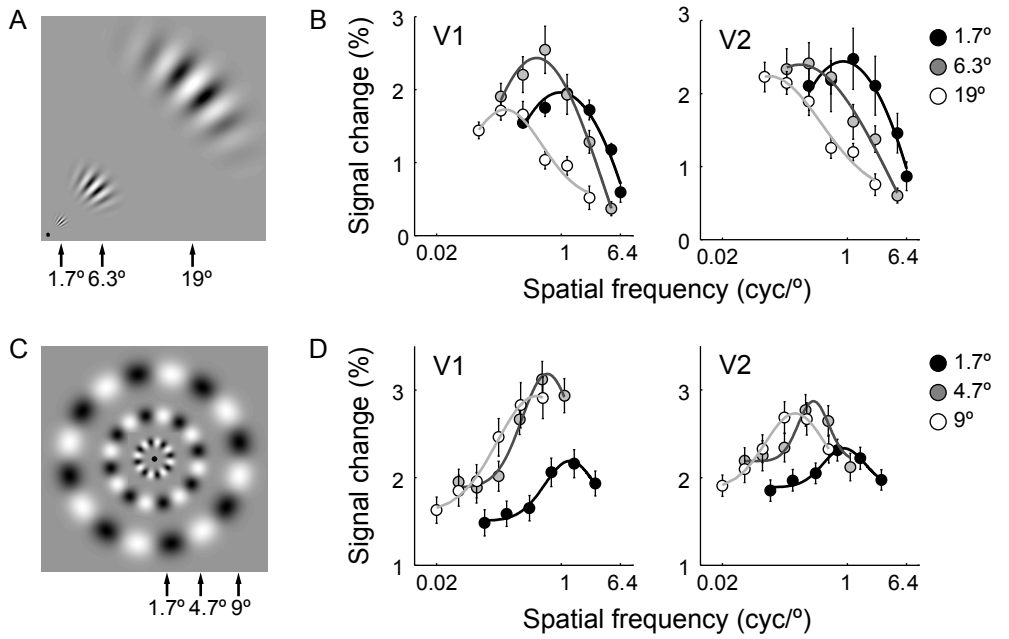

Figure 17: *Spatial frequency tuning in human visual cortex (Publication IV). A) The fMRI responses were measured to angular grating stimuli using a range of different spatial frequencies in a block design. Different visual field eccentricities were studied in subsequent experimental runs. B) The fMRI spatial frequency tuning curves (averaged across eight subjects) measured with the quadrant stimulus at three different eccentricities (A) are shown for visual areas V1 and V2. C) The ring stimulus and quadrant (A) stimulus provided complementary results. Ring stimulus enabled the use of lower SFs than the quadrant. D) The fMRI spatial frequency tuning curves (averaged across subjects) measured with the ring stimulus (C) are shown for visual areas V1 and V2. Note the different visual field eccentricities and range of SFs in B and D.*

without loss of eccentric specificity (Mullen et al., 2005).

Publication IV shows that fMRI responses in several human visual areas are tuned for SF (see examples in Figure 17). In visual areas V1, V2, V3, VP (V3v), V4v (hV4) and V3A, the fMRI spatial frequency tuning curves were band-pass tuned. Both the visual field eccentricity and the visual area affected the spatial frequency that evoked the largest response. The SF optima were the highest in visual area V1 (Figures 17 and 18). In each visual area, the SF optima decreased as function of the visual field eccentricity. At similar visual field eccentricity, the SF optimum in area V2 was, on average,

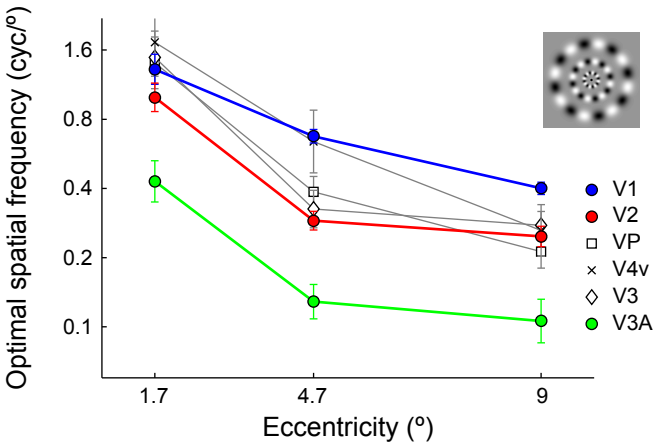

Figure 18: *The SF optima (peak of the SF tuning curve measured with fMRI) decreased in each visual area as function of the visual field eccentricity, and at similar visual field eccentricities, from V1 to V2 and from V2 to V3A. Note the logarithmic scale.*

two-thirds of the SF optimum in area V1 and approximately an equal shift to a lower SF preference was observed from area V2 to area V3A. The difference in the SF tuning between V1 and V2 was replicated in control experiments (see Publication IV). These findings that both the visual field eccentricity and the visual area affect the SF tuning are in agreement with the data from macaque monkeys (Schiller et al., 1976; De Valois et al., 1982; Foster et al., 1985). However, in macaques, area V3 shows preference for lower SFs than area V2 (Gegenfurtner et al., 1997). In our data the SF tuning was similar in V2 and V3 but differed between areas V2 and V3A. This is consistent with the view that human visual area V3A, rather than V3, is the most likely homologue to macaque area V3 (Tootell et al., 1997).

The optimal spatial frequencies (f_{opt}) can be converted to optimal spatial wavelengths ($\lambda_{\mathrm{opt}} = 1/f_{\mathrm{opt}}$). Publication IV estimated the cortical representations for the optimal spatial wavelengths in V1 using the estimate of cortical magnification within human V1 (Duncan and Boynton, 2003). Even though the SF optimum decreased as function of visual field eccentricity (from 1.2 cyc/deg at eccentricity of 1.7 deg to 0.18 cyc/deg at eccentricity of 19 deg) the corresponding measures of optimal spatial wavelengths on the cortical surface remained approximately constant across eccentricity (ca. 4–5 mm). This constant may reflect the extent of the horizontal connections that shape the spatial summation field of V1 neurons (Angelucci et al., 2002) and thus restrict the selective representation of low SFs. The decrease in the SF

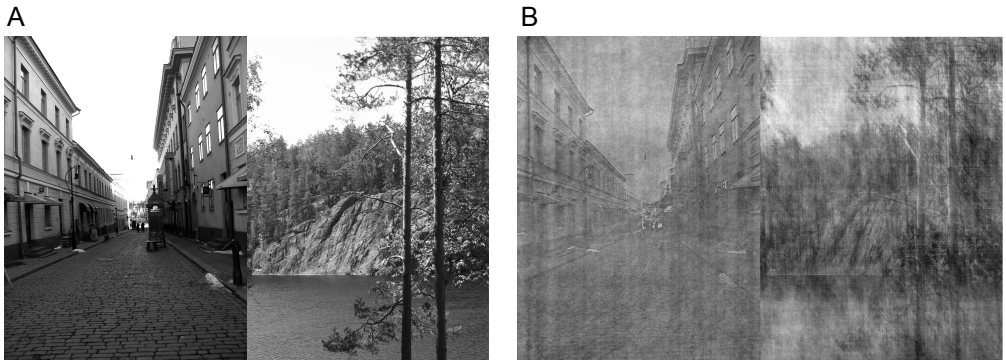

Figure 19: *Phase spectrum dominates perception in natural images. A) Two natural images. B) The amplitude spectra of the two images in A were exchanged. The hybrid image resembles the image from which the phase spectrum was taken.*

optima from V1 to V2 and from V2 to V3A is compatible with the view that early visual areas represent visual information at different spatial scales (Kourtzi et al., 2003; Hegde and Van Essen, 2007).

4.5 Sensitivity to cross-frequency phase relations in human visual cortex (Publication V)

Phase information in natural images

An image can be decomposed into a sum of sinusoidal components of different orientations, spatial frequencies, amplitudes and phases. Figure 19 illustrates the relative importance of the global phase and amplitude spectrum for perception. The phase spectrum dominates. Scrambling the phase structure of images effectively attenuates both the perception and the fMRI responses from the object-processing areas (Malach et al., 1995).

Visual features are perceived at locations of maximal local phase coherence (Morrone and Burr, 1988). A step edge (square wave) is an example of a visual feature with maximal local phase coherence across spatial frequency bands. It can be constructed from a series of sinusoidal waves

$$s(x) = \sum_{n=0}^{N} \frac{1}{2n+1} \sin((2n+1)x + \phi), \tag{5}$$

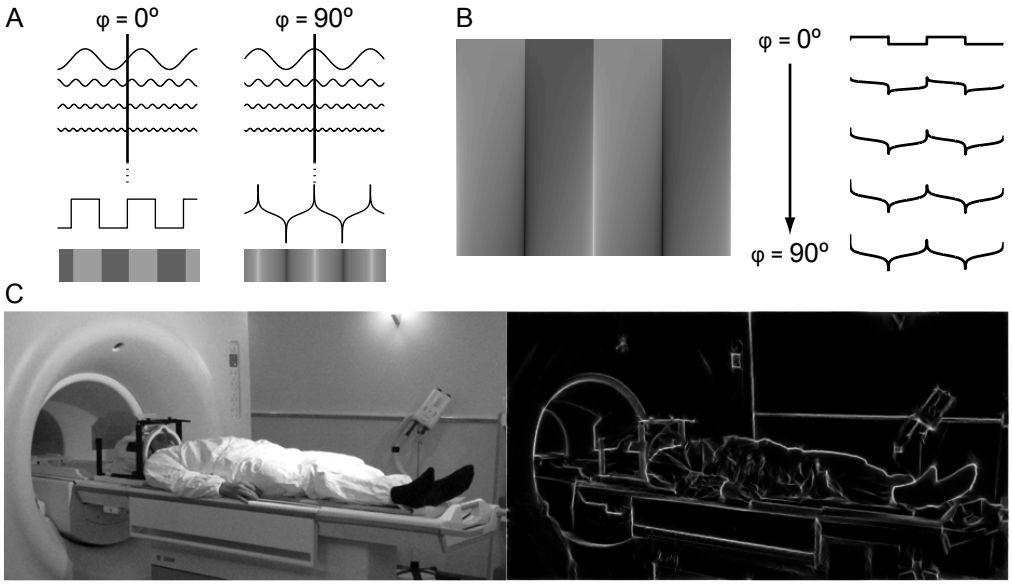

Figure 20: *Phase congruency at any phase value ϕ creates a salient feature in the image. A) A step edge (or square wave) can be constructed from a series of sinusoidal waves according to Equation 5 when $\phi = 0°$ and a line-like feature when $\phi = 90°$. B) Continuously varying the phase value ϕ from $0°$ to $90°$ creates a continuum of salient features at the location of the congruence phase. C) Important visual features can be detected based on the phase congruency across spatial frequency bands. The phase congruency map was calculated with the method developed by Kovesi (1999).*

where x denotes location and ϕ is a phase shift. The phase shift equals $0°$ in the case of a step edge, but actually the summation of sinusoidal waves according to Equation 5 results in a salient feature at the location of the local congruence phase ϕ at any phase value (Figure 20A,B; Kovesi, 1999). Phase congruency can be used for edge detection in natural images (Figure 20C; Morrone and Burr, 1988; Kovesi, 1999).

Computational model predicts pooling of spatial frequency bands

The behavior of simple cells in the V1 cortex can be described as spatiotemporal filters (Jones and Palmer, 1987; Ringach, 2002), which decompose the visual input into spatially localized and oriented spatial frequency components. Edges in natural images are not limited to separate narrow spatial frequency bands, but realistic edges are typically sharp broadband edges that require phase-sensitive pooling of different spatial frequencies (Griffin et

al., 2004). A natural broadband edge with local phase coherence across spatial frequency bands (Figure 20A,B) thus excites a number of V1 cells with different spatial frequency preferences and similar spatial phase preference.

Local energy model employs a pair of V1-like spatiotemporal filters to detect features based on the phase congruence across spatial frequency bands (Morrone and Burr, 1988). Although cells in V1 might detect some phase congruencies (Morrone and Burr, 1988; Mechler et al., 2002), it is likely that such features are mainly processed in the areas beyond V1. A computational study on natural image statistics suggested that the outputs from the primary visual cortex (V1) are optimally analyzed by pooling different spatial frequency bands together to represent these broadband edges (Hyvärinen et al., 2005).

Cortical sensitivity to phase difference between different spatial frequencies (Publication V)

Publication V studied phase-sensitive fMRI responses to find out how the human visual system encodes phase alignments across different spatial frequencies. The cortical sensitivity to phase difference between two different spatial frequencies was measured using an fMRI adaptation design. With adaptation we could assess the neural selectivities of overlapping neural populations (Fang et al., 2005).

The stimuli were constructed from two sinusoidal gratings (Figure 21A)

$$s(x) = \sin(x) + \frac{1}{3}\sin(3x + \phi), \tag{6}$$

where phase difference between the component gratings was changed by changing the absolute phase (ϕ) of the higher frequency grating. See Publication V for control measurements on changes in local contrast and position. The subjects were adapted to a compound grating where ϕ was either 0° or 180° (Figure 21B) and the responses were measured for compound gratings where ϕ was 0°, 45°, 90°, 135°, or 180°.

The fMRI signals showed a monotonic increase as function of the phase difference from the adaptation condition in several visual areas (Figure 21C). The fMRI data cannot reveal whether the adaptation effects and the observed sensitivity to spatial phase relations originates in V1 or in a higher-level visual area that provides feedback to the early areas. However, the data do imply

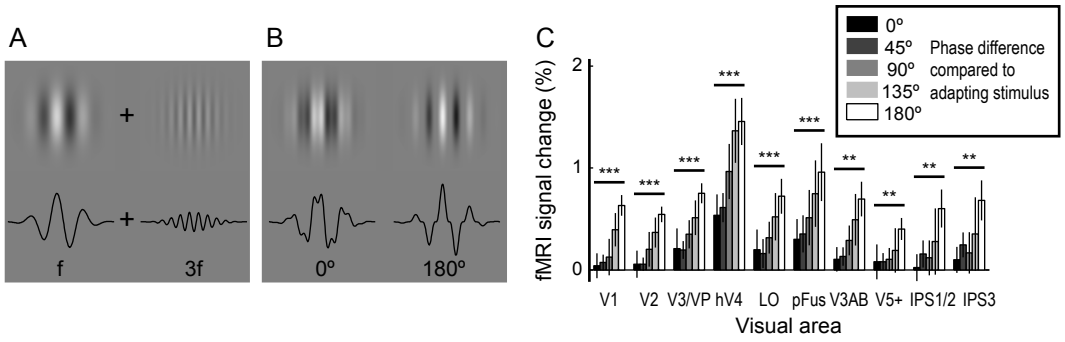

Figure 21: *Cortical sensitivity for cross-frequency phase difference (Publication V). A) fMRI adaptation design comprised compound grating stimuli with two spatial frequency components (f = 0.4 cyc/deg and 3f = 1.2 cyc/deg). B) The phase difference between the two spatial frequencies was in the adaptation stimulus either* 0° *or* 180°*. In the test stimuli, the phase difference was varied between* 0°*,* 45°*,* 90°*,* 135°*, and* 180° *(see Publication V). C) All studied visual areas showed an increase in the fMRI response as function of the phase difference from the adaptation stimulus (***p < 0.001, **p < 0.01; Page's L test). The mean fMRI responses from regions-of-interest in different visual areas are averaged across eight subjects.*

that human visual areas contain populations of neurons that compute the phase difference between different spatial frequencies.

Cortical representation of phase congruence (Publication V)

Based on the perceptual importance of phase congruency (Figure 20), Publication V also examined the possibility that phase congruency across spatial frequencies is encoded in the visual cortex. The stimuli were constructed from five sinusoidal gratings. The gratings were summed either with local phase coherence across frequency components (see Equation 5) or with random phase differences. The stimuli were presented in a block design with the congruent stimuli presented in one block and the random stimuli in another block (see example stimuli in Figure 22A).

All studied visual areas showed a stronger response for the stimuli with congruent phase structure. To compare responses in different visual areas, a phase congruency selectivity index (SI) was calculated

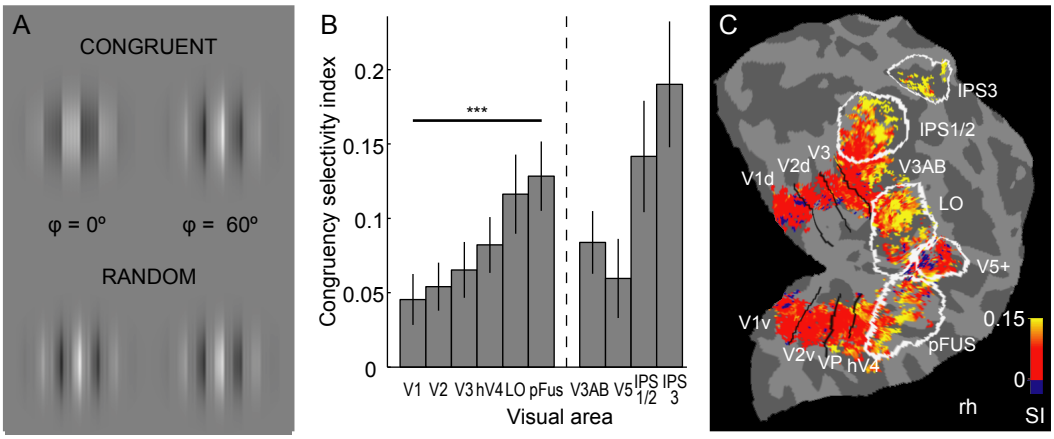

Figure 22: *Phase congruency selectivity in human visual cortex (Publication V). A) fMRI block experiment comprised compound grating stimuli (f = 0.4 cyc/deg, 3f, 5f, 7f, 9f) with congruent or random phase structure. B) All studied visual areas showed stronger response for the congruent stimuli with a gradual increase in the phase congruency selectivity index (SI, see Equation 7) along the ventral stream from V1 to pFus (***$p < 0.001$; Page's L test). The selectivity indexes from regions-of-interest in different visual areas are averaged across seven subjects. C) The topography of phase congruency selectivity is illustrated with a group-averaged SI map. The average cortical surface of the right hemisphere was created from the anatomical data of ten subjects and the functional data were resampled and averaged to the average cortical surface (Fischl et al., 1999b).*

$$SI = \frac{R_{\text{cong}} - R_{\text{rand}}}{R_{\text{cong}} + R_{\text{rand}}}, \tag{7}$$

where R_{cong} is the fMRI % signal change for the stimuli with congruent phase structure and R_{rand} the fMRI % signal change for the stimuli with random phase structure. This index increased through the ventral stream areas V1, V2, V3, hV4, LO and pFus and was high also in the dorsal stream areas along the intraparietal sulcus (Figure 22). These result suggests that the higher-level visual areas integrate the bandpass spatial frequency information from the low-level visual areas to represent natural broadband visual features with coherent phase structure.

5 Discussion and conclusions

This Thesis aimed at developing a novel retinotopic mapping method based on multifocal stimulation and at contributing to our understanding on the functional organization and plasticity of the human visual cortex.

The novel stimulation method for the characterization of visual field representations in human visual cortex was provided in Publication I. Compared to the existing method, the phase-encoded retinotopic mapping (Engel et al., 1994; Sereno et al., 1995; Warnking et al., 2002), multifocal fMRI provides a more straightforward analysis and interpretation of the retinotopic responses. Because the data analysis can be practically automated and the retinotopic organization can be visualized on the subject's anatomical MRI, multifocal fMRI has potential also for clinical use. Multifocal fMRI has already been applied to the localization of V1 before neurosurgery. Preoperative mapping of early visual areas could reduce the risk of cortical blindness following occipital surgery.

It remains to be seen to what extent multifocal fMRI can compete with the phase-encoded retinotopic mapping. Recently, the advances in the phase-encoded method combined with the improvements in the imaging techniques have revealed retinotopic organization in several higher-level visual areas (Wandell et al., 2007; Saygin and Sereno, 2008; Arcaro et al., 2009), from where we have not been able to map retinotopic multifocal responses. In the higher-level visual areas, the retinotopic responses for the phase-encoded stimulus can be enhances with a task that engage subject's attention to the stimulated part of the visual field (Saygin and Sereno, 2008). The spatial layout of the multifocal stimulus appears random to the subject, which complicates the spatially specific direction of attention to the stimulated regions.

Publication II showed that the multifocal fMRI responses are suppressed already in the primary visual cortex due to the parallel stimulation of the multiple stimulus regions and that this suppression most likely is of neural origin. Hence, the main limitation of the multifocal fMRI is that it is not easily applied to the retinotopic mapping of the higher-level visual areas, where the cells have large receptive fields and show pronounced nonlinearities in the spatial summation within the receptive field (Kastner et al., 2001). However, with recent developments, multifocal fMRI is well-suited for retinotopic mapping in visual areas V1–V3AB/hV4 and has proven to be a very useful tool as a functional localizer of retinotopic regions-of-interest.

Publication III showed that adult visual cortex is capable of large-scale reorganization. In this case study, the subject was an adult patient with a chronic visual field defect due to a lesion in the visual cortex. He attended intensive training of visual functions in the blind hemifield (Raninen et al., 2007). Recent cumulative evidence shows that vision in cortically blind patients can be improved with training (for reviews, see Sahraie, 2007; Huxlin, 2008). The most effective training for cortical blindness appears to be intensive training of the residual vision deep within the blind hemifield (Sahraie et al., 2006; Raninen et al., 2007; Jobke et al., 2009). Publication III together with Raninen et al. (2007) showed that the improved visual performance can be associated with reorganization of the visual cortex. The trained (right) hemifield was represented in multiple visual areas in the healthy (right) hemisphere. There is now clear evidence that the adult visual cortex can reorganize after damage to different parts of the visual system, including the retina (Baker et al., 2008), the fibers that provide input to V1 (Dilks et al., 2007), and the primary visual cortex (Publication III; for a review, see Huxlin, 2008).

The main limitation in studies on plasticity in adult visual cortex and on training-induced changes in visual processing is that they typically comprise only a few patients. In Publication III, the result was very clear, but we cannot argue that similar large-scale reorganization would be evident in every patient enrolling in the training. In fact, in another patient, who participated in similar training but was not eligible for fMRI experiments, the topography of evoked neuromagnetic responses for the trained hemifield was very different and suggested recruitment of extrastriate visual areas in the lesioned hemisphere (Raninen et al., 2007). This topic would deserve a large-scale population study testing the generalization of training-induced plasticity in the adult visual system.

Tuning curves are widely used in electrophysiological studies to describe a neuron's response to a particular stimulus parameter, such as the orientation or spatial frequency of a visual stimulus. Because the coupling between neural activity and the fMRI response is incompletely understood, comparison of fMRI and neural tuning curves can provide an important link between the single-cell responses and the indirect measure of the neural population response measured with fMRI. Publication IV presented fMRI tuning curves for spatial frequency measured in several human visual areas. Overall, the fMRI tuning curves in different visual field eccentricities and visual areas had similarities with the neural tuning curves reported in monkeys (Schiller et al., 1976; De Valois et al., 1982; Foster et al., 1985; Gegenfurtner et al., 1997).

The fMRI tuning curves for spatial frequency were bandpass in visual areas V1–V3, hV4, and V3A with the peak frequency decreasing progressively between areas V1, V2 and V3A (Publication IV). This result, together with known similarities in complex shape representations between early visual areas (Hegde and Van Essen, 2007) and the size-dependence of the integration of local features into global shapes (Kourtzi et al., 2003), support the view that early visual areas process visual information at different spatial scales. Within each area, the peak frequency decreased with increasing visual field eccentricity (Publication IV). However, when taking into account the cortical magnification within human V1 (Duncan and Boynton, 2003), the corresponding cortical representations, remained approximately constant across eccentricity. This measure was comparable to the extent of lateral connections within primate V1 (Angelucci et al., 2002). The lateral connections likely mediate the spatial summation of macaque V1 cells (Angelucci et al., 2002) and, therefore, our result could reflect the extent of spatial summation in human visual cortex.

Every patch in the visual field is analyzed by a population of V1 neurons that jointly represent, for example, the spatial frequency content of the input. A single neuron is sensitive only to a limited range of spatial frequencies. In natural images, features like step edges are, however, not limited to narrow spatial frequency bands. In fact, features are perceived at locations of maximal local phase congruency across spatial frequency bands (Morrone and Burr, 1988). This suggests that visual system should implement phase-sensitive pooling of spatial frequency information in the identification of natural broadband edges.

Publication V showed that phase relations in broadband visual stimuli are encoded in the human visual cortex. The fMRI adaptation design enabled the detection of phase-sensitive responses in several visual areas, including V1. By comparing responses to stimuli with congruent phase alignments to stimuli with random phase alignments, we showed that the selectivity to congruent phase structure increased in the hierarchy of the visual areas. These results suggest that phase-sensitive pooling of spatial frequencies takes place already in human V1, but only higher-level areas are capable of pooling spatial frequency information across spatial scales typical for broadband natural images.

The motivation for searching for pooling over spatial frequency in human visual cortex was originally derived from the statistics of natural images. A computational study on natural image statistics suggested that pooling

over spatial frequency is an optimal strategy to analyze the output from V1 (Hyvärinen et al., 2005). The functional organization in many visual areas, *e.g.*, area V2 (Boynton and Hegde, 2004), is still poorly understood. Computational modeling can provide us important novel predictions on cortical functions to be tested experimentally.

References

Andersson JL, Hutton C, Ashburner J, Turner R, Friston K (2001) Modeling geometric deformations in EPI time series. *NeuroImage* 13:903–19.

Angelucci A, Levitt JB, Walton EJ, Hupe JM, Bullier J, Lund JS (2002) Circuits for local and global signal integration in primary visual cortex. *J Neurosci* 22:8633–46.

Arcaro MJ, McMains SA, Singer BD, Kastner S (2009) Retinotopic organization of human ventral visual cortex. *J Neurosci* 29:10638–52.

Astafiev SV, Shulman GL, Stanley CM, Snyder AZ, Van Essen DC, Corbetta M, Van Essen DC (2003) Functional organization of human intraparietal and frontal cortex for attending, looking, and pointing. *J Neurosci* 23:4689–99.

Atick JJ, Redlich AN (1992) What does the retina know about natural scenes? *Neural Comput* 4:196–210.

Baillet S, Mosher J, Leahy R (2001) Electromagnetic brain mapping. *IEEE Signal Proc Mag* 18:14–30.

Baker CI, Dilks DD, Peli E, Kanwisher N (2008) Reorganization of visual processing in macular degeneration: replication and clues about the role of foveal loss. *Vision Res* 48:1910–9.

Baker CI, Peli E, Knouf N, Kanwisher NG (2005) Reorganization of visual processing in macular degeneration. *J Neurosci* 25:614–8.

Balliet R, Blood KM, Bach-y-Rita P (1985) Visual field rehabilitation in the cortically blind? *J Neurol Neurosur Ps* 48:1113–24.

Barone P, Batardiere A, Knoblauch K, Kennedy H (2000) Laminar distribution of neurons in extrastriate areas projecting to visual areas V1 and V4 correlates with the hierarchical rank and indicates the operation of a distance rule. *J Neurosci* 20:3263–81.

Baseler HA, Morland AB, Wandell BA (1999) Topographic organization of human visual areas in the absence of input from primary cortex. *J Neurosci* 19:2619–27.

Baseler HA, Sutter EE, Klein SA, Carney T (1994) The topography of visual evoked response properties across the visual field. *Electroencephalogr Clin Neurophysiol* 90:65–81.

Bittar RG, Ptito M, Faubert J, Dumoulin SO, Ptito A (1999) Activation of the remaining hemisphere following stimulation of the blind hemifield in hemispherectomized subjects. *NeuroImage* 10:339–46.

Blake DT, Heiser MA, Caywood M, Merzenich MM (2006) Experience-dependent adult cortical plasticity requires cognitive association between sensation and reward. *Neuron* 52:371–81.

Bloch F, Hansen WW, Packard M (1946) The nuclear induction experiment. *Phys Rev* 70:474–85.

Boynton GM, Hegde J (2004) Visual cortex: the continuing puzzle of area V2. *Curr Biol* 14:R523–4.

Brewer AA, Liu J, Wade AR, Wandell BA (2005) Visual field maps and stimulus selectivity in human ventral occipital cortex. *Nat Neurosci* 8:1102–9.

Bridge H, Thomas O, Jbabdi S, Cowey A (2008) Changes in connectivity after visual cortical brain damage underlie altered visual function. *Brain* 131:1433–44.

Bullier J, Girard P, Salin PA (1994) The role of area 17 in the transfer of information to extrastriate visual cortex. *Cerebral Cortex* 10:301–330.

Carandini M, Demb JB, Mante V, Tolhurst DJ, Dan Y, Olshausen BA, Gallant JL, Rust NC (2005) Do we know what the early visual system does? *J Neurosci* 25:10577–97.

Cavanaugh JR, Bair W, Movshon JA (2002a) Nature and interaction of signals from the receptive field center and surround in macaque V1 neurons. *J Neurophysiol* 88:2530–46.

Cavanaugh JR, Bair W, Movshon JA (2002b) Selectivity and spatial distribution of signals from the receptive field surround in macaque V1 neurons. *J Neurophysiol* 88:2547–56.

Chen X, Han F, Poo MM, Dan Y (2007) Excitatory and suppressive receptive field subunits in awake monkey primary visual cortex (V1). *P Natl Acad Sci USA* 104:19120–5.

Curcio CA, Sloan KR, Kalina RE, Hendrickson AE (1990) Human photoreceptor topography. *J Comp Neurol* 292:497–523.

Dale AM, Fischl B, Sereno MI (1999) Cortical surface-based analysis. I. Segmentation and surface reconstruction. *NeuroImage* 9:179–94.

Daniel PM, Whitteridge D (1961) The representation of the visual field on the cerebral cortex in monkeys. *J Physiol* 159:203–221.

De Valois RL, Albrecht DG, Thorell LG (1982) Spatial frequency selectivity of cells in macaque visual cortex. *Vision Res* 22:545–59.

Dilks DD, Serences JT, Rosenau BJ, Yantis S, McCloskey M (2007) Human adult cortical reorganization and consequent visual distortion. *J Neurosci* 27:9585–94.

Dougherty RF, Koch VM, Brewer AA, Fischer B, Modersitzki J, Wandell BA (2003) Visual field representations and locations of visual areas V1/2/3 in human visual cortex. *J Vision* 3:586–98.

Dumoulin SO, Wandell BA (2008) Population receptive field estimates in human visual cortex. *NeuroImage* 39:647–60.

Duncan RO, Boynton GM (2003) Cortical magnification within human primary visual cortex correlates with acuity thresholds. *Neuron* 38:659–71.

Engel S, Rumelhart D, Wandell B, Lee A, Glover G, Chichilnisky E, Shadlen M (1994) fMRI of human visual cortex. *Nature* 369:525.

Fang F, Murray SO, Kersten D, He S (2005) Orientation-tuned fMRI adaptation in human visual cortex. *J Neurophysiol* 94:4188–95.

Felleman DJ, Van Essen DC (1991) Distributed hierarchical processing in the primate cerebral cortex. *Cereb Cortex* 1:1–47.

Field GD, Chichilnisky EJ (2007) Information processing in the primate retina: circuitry and coding. *Annu Rev Neurosci* 30:1–30.

Fischl B, Sereno MI, Dale AM (1999a) Cortical surface-based analysis. II: Inflation, flattening, and a surface-based coordinate system. *NeuroImage* 9:195–207.

Fischl B, Sereno MI, Tootell RB, Dale AM (1999b) High-resolution intersubject averaging and a coordinate system for the cortical surface. *Hum Brain Mapp* 8:272–84.

Fitzpatrick D (2000) Seeing beyond the receptive field in primary visual cortex. *Curr Opin Neurobiol* 10:438–43.

Foster KH, Gaska JP, Nagler M, Pollen DA (1985) Spatial and temporal frequency selectivity of neurones in visual cortical areas V1 and V2 of the macaque monkey. *J Physiol* 365:331–63.

Fox PT, Raichle ME, Mintun MA, Dence C (1988) Nonoxidative glucose consumption during focal physiologic neural activity. *Science* 241:462–4.

Frackowiak R, Friston K, Frith C, Dolan R, Price C, Zeki S, Ashburner J, Penny W (2003) *Human Brain Function* San Diego: Academic Press, 2nd edition.

Friston KJ, Holmes AP, Worsley KJ, Poline JP, Frith CD, Frackowiak RSJ (1994) Statistical parametric maps in functional imaging: A general linear approach. *Hum Brain Mapp* 2:189–210.

Gegenfurtner KR, Kiper DC, Levitt JB (1997) Functional properties of neurons in macaque area V3. *J Neurophysiol* 77:1906–23.

Giaume C, Koulakoff A, Roux L, Holcman D, Rouach N (2010) Astroglial networks: a step further in neuroglial and gliovascular interactions. *Nat Rev Neurosci* 11:87–99.

Gilbert CD, Wiesel TN (1992) Receptive field dynamics in adult primary visual cortex. *Nature* 356:150–2.

Gilhotra JS, Mitchell P, Healey PR, Cumming RG, Currie J (2002) Homonymous visual field defects and stroke in an older population. *Stroke* 33:2417–20.

Goense JB, Logothetis NK (2006) Laminar specificity in monkey V1 using high-resolution SE-fMRI. *Magn Reson Imaging* 24:381–92.

Goense JB, Logothetis NK (2008) Neurophysiology of the BOLD fMRI signal in awake monkeys. *Curr Biol* 18:631–40.

Goodale MA, Milner AD (1992) Separate visual pathways for perception and action. *Trends Neurosci* 15:20–5.

Griffin LD, Lillholm M, Nielsen M (2004) Natural image profiles are most likely to be step edges. *Vision Res* 44:407–21.

Grill-Spector K, Kourtzi Z, Kanwisher N (2001) The lateral occipital complex and its role in object recognition. *Vision Res* 41:1409–22.

Grill-Spector K, Kushnir T, Edelman S, Avidan G, Itzchak Y, Malach R (1999) Differential processing of objects under various viewing conditions in the human lateral occipital complex. *Neuron* 24:187–203.

Grill-Spector K, Malach R (2004) The human visual cortex. *Annu Rev Neurosci* 27:649–77.

Grinvald A, Lieke EE, Frostig RD, Hildesheim R (1994) Cortical point-spread function and long-range lateral interactions revealed by real-time optical imaging of macaque monkey primary visual cortex. *J Neurosci* 14:2545–68.

Hadjikhani N, Liu AK, Dale AM, Cavanagh P, Tootell RB (1998) Retinotopy and color sensitivity in human visual cortical area V8. *Nat Neurosci* 1:235–41.

Hagmann P, Kurant M, Gigandet X, Thiran P, Wedeen VJ, Meuli R, Thiran JP (2007) Mapping human whole-brain structural networks with diffusion MRI. *PLoS ONE* 2:e597.

Harel N, Uğurbil K, Uludağ K, Yacoub E (2006) Frontiers of brain mapping using MRI. *J Magn Reson Imaging* 23:945–57.

Haxby JV, Gobbini MI, Furey ML, Ishai A, Schouten JL, Pietrini P (2001) Distributed and overlapping representations of faces and objects in ventral temporal cortex. *Science* 293:2425–30.

Haydon PG, Carmignoto G (2006) Astrocyte control of synaptic transmission and neurovascular coupling. *Physiol Rev* 86:1009–31.

Hegde J, Van Essen DC (2007) A comparative study of shape representation in macaque visual areas V2 and V4. *Cereb Cortex* 17:1100–16.

Hendry SH, Reid RC (2000) The koniocellular pathway in primate vision. *Annu Rev Neurosci* 23:127–53.

Holmes G (1918) Disturbances of vision by cerebral lesions. *Brit J Ophthalmol* 2:353–84.

Hood DC (2000) Assessing retinal function with the multifocal technique. *Prog Retin Eye Res* 19:607–46.

Horton JC (2005) Disappointing results from Nova Vision's visual restoration therapy. *Brit J Ophthalmol* 89:1–2.

Horton JC, Hoyt WF (1991a) Quadrantic visual field defects. A hallmark of lesions in extrastriate (V2/V3) cortex. *Brain* 114:1703–18.

Horton JC, Hoyt WF (1991b) The representation of the visual field in human striate cortex. A revision of the classic Holmes map. *Arch Ophthal-*

mol 109:816–24.

Hubel D, Wiesel T (1962) Receptive fields, binocular interaction and functional architecture in the cat's visual cortex. *J Physiol* 160:106–54.

Hubel D, Wiesel T (1968) Receptive fields and functional architecture of monkey striate cortex. *J Physiol* 195:215–43.

Huettel S, Song AW, McCarthy G (2004) *Functional Magnetic Resonance Imaging.* Sunderland, MA: Sinauer Associates.

Huk AC, Dougherty RF, Heeger DJ (2002) Retinotopy and functional subdivision of human areas MT and MST. *J Neurosci* 22:7195–205.

Huxlin KR (2008) Perceptual plasticity in damaged adult visual systems. *Vision Res* 48:2154–2166.

Huxlin K, Martin T, Kelly K, Riley M, Friedman D, Burgin W, Hayhoe M (2009) Perceptual Relearning of Complex Visual Motion after V1 Damage in Humans. *J Neurosci* 29:3981–91.

Hyvärinen A, Gutmann M, Hoyer PO (2005) Statistical model of natural stimuli predicts edge-like pooling of spatial frequency channels in V2. *BMC Neurosci* 6:12.

Hyvärinen A, Hoyer P (2000) Emergence of phase- and shift-invariant features by decomposition of natural images into independent feature subspaces. *Neural Comput* 12:1705–20.

Hyvärinen A, Hurri J, Hoyer PO (2009) *Natural Image Statistics — A Probabilistic Approach to Early Computational Vision.* London: Springer.

Hyvärinen L, Raninen AN, Näsänen R (2002) Vision rehabilitation in homonymous hemianopia. *Neuro-Ophthalmology* 27:97–102.

Hämäläinen M, Hari R, Ilmoniemi RJ, Knuutila J, Lounasmaa OV (1993) Magnetoencephalography—theory, instrumentation, and applications to noninvasive studies of the working human brain. *Rev Mod Phys* 65:413–97.

Issa NP, Trepel C, Stryker MP (2000) Spatial frequency maps in cat visual cortex. *J Neurosci* 20:8504–14.

James AC (2003) The pattern-pulse multifocal visual evoked potential. *Invest Ophth Vis Sci* 44:879–90.

Jobke S, Kasten E, Sabel BA (2009) Vision restoration through extrastriate stimulation in patients with visual field defects: a double-blind and randomized experimental study. *Neurorehab Neural Re* 23:246–55.

Jones JP, Palmer LA (1987) An evaluation of the two-dimensional Gabor filter model of simple receptive fields in cat striate cortex. *J Neurophysiol* 58:1233–58.

Julkunen L, Tenovuo O, Jääskeläinen S, Hämäläinen H (2003) Rehabilitation of chronic post-stroke visual field defect with computer-assisted training: a clinical and neurophysiological study. *Restor Neurol Neuros* 21:19–28.

Kaas JH, Krubitzer LA, Chino YM, Langston AL, Polley EH, Blair N (1990)

Reorganization of retinotopic cortical maps in adult mammals after lesions of the retina. *Science* 248:229–31.

Kanwisher N, McDermott J, Chun MM (1997) The fusiform face area: a module in human extrastriate cortex specialized for face perception. *J Neurosci* 17:4302–11.

Kasten E, Wüst S, Behrens-Baumann W, Sabel BA (1998) Computer-based training for the treatment of partial blindness. *Nat Med* 4:1083–7.

Kastner S, De Weerd P, Pinsk MA, Elizondo MI, Desimone R, Ungerleider LG (2001) Modulation of sensory suppression: implications for receptive field sizes in the human visual cortex. *J Neurophysiol* 86:1398–411.

Kerkhoff G, Münssinger U, Haaf E, Eberle-Strauss G, Stögerer E (1992) Rehabilittion of homonymous scotomata in patients with postgeniculate damage of the visual system: saccadic compensation training. *Restor Neurol Neuros* 4:245–54.

Kobatake E, Tanaka K (1994) Neuronal selectivities to complex object features in the ventral visual pathway of the macaque cerebral cortex. *J Neurophysiol* 71:856–67.

Konen CS, Kastner S (2008) Two hierarchically organized neural systems for object information in human visual cortex. *Nat Neurosci* 11:224–31.

Kourtzi Z, Tolias AS, Altmann CF, Augath M, Logothetis NK (2003) Integration of local features into global shapes: monkey and human fMRI studies. *Neuron* 37:333–46.

Kovesi P (1999) Image features from phase congruency. *Videre: A Journal of Computer Vision Research* 1:1–26.

Lanyon LJ, Giaschi D, Young SA, Fitzpatrick K, Diao L, Bjornson BH, Barton JJ (2009) Combined functional MRI and diffusion tensor imaging analysis of visual motion pathways. *J Neuro-ophthalmol* 29:96–103.

Larsson J, Heeger DJ (2006) Two retinotopic visual areas in human lateral occipital cortex. *J Neurosci* 26:13128–42.

Laughlin SB (1989) The role of sensory adaptation in the retina. *J Exp Biol* 146:39–62.

Leh SE, Chakravarty MM, Ptito A (2008) The connectivity of the human pulvinar: a diffusion tensor imaging tractography study. *Int J Biomed Imaging* doi:10.1155/2008/789539.

Leh SE, Johansen-Berg H, Ptito A (2006) Unconscious vision: new insights into the neuronal correlate of blindsight using diffusion tractography. *Brain* 129:1822–32.

Lennie P, Movshon JA (2005) Coding of color and form in the geniculostriate visual pathway (invited review). *J Opt Soc Am A* 22:2013–33.

Liepert J, Bauder H, Wolfgang HR, Miltner WH, Taub E, Weiller C (2000) Treatment-induced cortical reorganization after stroke in humans.

Stroke 31:1210–6.

Liu TT (2004) Efficiency, power, and entropy in event-related fMRI with multiple trial types. Part II: design of experiments. *NeuroImage* 21:401–13.

Logothetis NK (2008) What we can do and what we cannot do with fMRI. *Nature* 453:869–78.

Logothetis NK, Pauls J, Augath M, Trinath T, Oeltermann A (2001) Neurophysiological investigation of the basis of the fMRI signal. *Nature* 412:150–7.

Logothetis NK, Wandell BA (2004) Interpreting the BOLD signal. *Annu Rev Physiol* 66:735–69.

Malach R, Reppas JB, Benson RR, Kwong KK, Jiang H, Kennedy WA, Ledden PJ, Brady TJ, Rosen BR, Tootell RB (1995) Object-related activity revealed by functional magnetic resonance imaging in human occipital cortex. *P Natl Acad Sci USA* 92:8135–9.

McKeefry DJ, Zeki S (1997) The position and topography of the human colour centre as revealed by functional magnetic resonance imaging. *Brain* 120:2229–42.

Mechler F, Reich DS, Victor JD (2002) Detection and discrimination of relative spatial phase by V1 neurons. *J Neurosci* 22:6129–57.

Merzenich MM, Nelson RJ, Stryker MP, Cynader MS, Schoppmann A, Zook JM (1984) Somatosensory cortical map changes following digit amputation in adult monkeys. *J Comp Neurol* 224:591–605.

Morrone MC, Burr DC (1988) Feature detection in human vision: a phase-dependent energy model. *P Roy Soc Lond B Bio* 235:221–45.

Mountcastle VB (1997) The columnar organization of the neocortex. *Brain* 120:701–22.

Movshon JA, Thompson ID, Tolhurst DJ (1978) Spatial summation in the receptive fields of simple cells in the cat's striate cortex. *J Physiol* 283:53–77.

Mullen KT, Sakurai M, Chu W (2005) Does l/m cone opponency disappear in human periphery? *Perception* 34:951–9.

Nelles G, Esser J, Eckstein A, Tiede A, Gerhard H, Diener HC (2001) Compensatory visual field training for patients with hemianopia after stroke. *Neurosci Lett* 306:189–92.

Nudo RJ, Milliken GW (1996) Reorganization of movement representations in primary motor cortex following focal ischemic infarcts in adult squirrel monkeys. *J Neurophysiol* 75:2144–9.

Ogawa S, Lee TM, Kay AR, Tank DW (1990) Brain magnetic resonance imaging with contrast dependent on blood oxygenation. *P Natl Acad Sci USA* 87:9868–72.

Ogawa S, Tank DW, Menon R, Ellermann JM, Kim SG, Merkle H, Ugurbil K (1992) Intrinsic signal changes accompanying sensory stimulation: func-

tional brain mapping with magnetic resonance imaging. *P Natl Acad Sci USA* 89:5951–5.

Olman CA, Inati S, Heeger DJ (2007) The effect of large veins on spatial localization with GE BOLD at 3 T: Displacement, not blurring. *NeuroImage* 34:1126–35.

Olshausen BA, Field DJ (1996) Emergence of simple-cell receptive field properties by learning a sparse code for natural images. *Nature* 381:607–9.

Orban GA (2008) Higher order visual processing in macaque extrastriate cortex. *Physiol. Rev.* 88:59–89.

Parkes LM, Schwarzbach JV, Bouts AA, Deckers RH, Pullens P, Kerskens CM, Norris DG (2005) Quantifying the spatial resolution of the gradient echo and spin echo BOLD response at 3 Tesla. *Magn Reson Med* 54:1465–72.

Pitzalis S, Galletti C, Huang RS, Patria F, Committeri G, Galati G, Fattori P, Sereno MI (2006) Wide-field retinotopy defines human cortical visual area V6. *J Neurosci* 26:7962–73.

Pitzalis S, Sereno MI, Committeri G, Fattori P, Galati G, Patria F, Galletti C (2010) Human V6: the medial motion area. *Cereb Cortex* 20:411–24.

Polimeni JR, Balasubramanian M, Schwartz EL (2006) Multi-area visuotopic map complexes in macaque striate and extra-striate cortex. *Vision Res* 46:3336–59.

Pommerenke K, Markowitsch H (1989) Rehabilitation training of homonymous visual field defects in patients with postgeniculate damage of the visual system. *Restor Neurol Neurosci* 1:47–63.

Pons TP, Garraghty PE, Ommaya AK, Kaas JH, Taub E, Mishkin M (1991) Massive cortical reorganization after sensory deafferentation in adult macaques. *Science* 252:1857–60.

Ptito M, Johannsen P, Faubert J, Gjedde A (1999) Activation of human extrageniculostriate pathways after damage to area V1. *NeuroImage* 9:97–107.

Rabi II, Zacharias JR, Millman S, Kusch P (1938) A new method of measuring nuclear magnetic moment. *Phys Rev* 53:318.

Raichle ME, Mintun MA (2006) Brain work and brain imaging. *Annu Rev Neurosci* 29:449–76.

Raninen A, Vanni S, Hyvärinen L, Näsänen R (2007) Temporal sensitivity in a hemianopic visual field can be improved by long-term training using flicker stimulation. *J Neurol Neurosur Ps* 78:66–73.

Ringach DL (2002) Spatial structure and symmetry of simple-cell receptive fields in macaque primary visual cortex. *J Neurophysiol* 88:455–63.

Rossini PM, Calautti C, Pauri F, Baron JC (2003) Post-stroke plastic reorganisation in the adult brain. *Lancet Neurol* 2:493–502.

Rust NC, Schwartz O, Movshon JA, Simoncelli EP (2005) Spatiotemporal elements of macaque V1 receptive fields. *Neuron* 46:945–56.

Saalmann YB, Kastner S (2009) Gain control in the visual thalamus during perception and cognition. *Curr Opin Neurobiol* 19:408–14.

Sabel BA, Kenkel S, Kasten E (2004) Vision restoration therapy (VRT) efficacy as assessed by comparative perimetric analysis and subjective questionnaires. *Restor Neurol Neuros* 22:399–420.

Sahraie A (2007) Induced visual sensitivity changes in chronic hemianopia. *Curr Opin Neurol* 20:661–6.

Sahraie A, Trevethan CT, MacLeod MJ, Murray AD, Olson JA, Weiskrantz L (2006) Increased sensitivity after repeated stimulation of residual spatial channels in blindsight. *P Natl Acad Sci USA* 103:14971–6.

Saxe R, Brett M, Kanwisher N (2006) Divide and conquer: a defense of functional localizers. *NeuroImage* 30:1088–96.

Saygin AP, Sereno MI (2008) Retinotopy and attention in human occipital, temporal, parietal, and frontal cortex. *Cereb Cortex* 18:2158–68.

Sayres R, Grill-Spector K (2008) Relating retinotopic and object-selective responses in human lateral occipital cortex. *J Neurophysiol* 100:249–67.

Schiller PH, Finlay BL, Volman SF (1976) Quantitative studies of single-cell properties in monkey striate cortex. III. Spatial frequency. *J Neurophysiol* 39:1334–51.

Schwartz EL (1980) Computational anatomy and functional architecture of striate cortex: a spatial mapping approach to perceptual coding. *Vision Res* 20:645–69.

Schwarzlose RF, Swisher JD, Dang S, Kanwisher N (2008) The distribution of category and location information across object-selective regions in human visual cortex. *P Natl Acad Sci USA* 105:4447–52.

Sereno MI, Dale AM, Reppas JB, Kwong KK, Belliveau JW, Brady TJ, Rosen BR, Tootell RB (1995) Borders of multiple visual areas in humans revealed by functional magnetic resonance imaging. *Science* 268:889–93.

Shulman RG, Hyder F, Rothman DL (2001) Cerebral energetics and the glycogen shunt: neurochemical basis of functional imaging. *P Natl Acad Sci USA* 98:6417–22.

Silver MA, Kastner S (2009) Topographic maps in human frontal and parietal cortex. *Trends Cogn Sci* 13:488–95.

Simoncelli EP, Olshausen BA (2001) Natural image statistics and neural representation. *Annu Rev Neurosci* 24:1193–216.

Smirnakis SM, Berry MJ, Warland DK, Bialek W, Meister M (1997) Adaptation of retinal processing to image contrast and spatial scale. *Nature* 386:69–73.

Smirnakis SM, Brewer AA, Schmid MC, Tolias AS, Schuz A, Augath M,

Inhoffen W, Wandell BA, Logothetis NK (2005) Lack of long-term cortical reorganization after macaque retinal lesions. *Nature* 435:300–7.

Stenbacka L, Vanni S (2007) fMRI of peripheral visual field representation. *Clin Neurophysiol* 118:1303–14.

Stoerig P, Cowey A (1997) Blindsight in man and monkey. *Brain* 120:535–59.

Sunness JS, Liu T, Yantis S (2004) Retinotopic mapping of the visual cortex using functional magnetic resonance imaging in a patient with central scotomas from atrophic macular degeneration. *Ophthalmology* 111:1595–8.

Swisher JD, Halko MA, Merabet LB, McMains SA, Somers DC (2007) Visual topography of human intraparietal sulcus. *J Neurosci* 27:5326–37.

Tootell RB, Mendola JD, Hadjikhani NK, Ledden PJ, Liu AK, Reppas JB, Sereno MI, Dale AM (1997) Functional analysis of V3A and related areas in human visual cortex. *J Neurosci* 17:7060–78.

Tootell RB, Mendola JD, Hadjikhani NK, Liu AK, Dale AM (1998) The representation of the ipsilateral visual field in human cerebral cortex. *P Natl Acad Sci USA* 95:818–24.

Tootell RB, Reppas JB, Kwong KK, Malach R, Born RT, Brady TJ, Rosen BR, Belliveau JW (1995) Functional analysis of human MT and related visual cortical areas using magnetic resonance imaging. *J Neurosci* 15:3215–30.

Tootell RB, Silverman MS, Switkes E, De Valois RL (1982) Deoxyglucose analysis of retinotopic organization in primate striate cortex. *Science* 218:902–4.

Ungerleider LG, Haxby JV (1994) 'What' and 'where' in the human brain. *Curr Opin Neurobiol* 4:157–65.

Van Essen DC (2004) Organization of visual areas in macaque and human cerebral cortex. In Chalupa L, Werner JS, editors, *The Visual Neurosciences*, pp. 507–21. MIT Press, Cambridge, MA, USA.

Van Essen DC, Newsome WT, Maunsell JH (1984) The visual field representation in striate cortex of the macaque monkey: asymmetries, anisotropies, and individual variability. *Vision Res* 24:429–48.

Wade A, Augath M, Logothetis N, Wandell B (2008) fMRI measurements of color in macaque and human. *J Vision* 8:1–19.

Wager TD, Nichols TE (2003) Optimization of experimental design in fMRI: a general framework using a genetic algorithm. *NeuroImage* 18:293–309.

Wandell BA, Dumoulin SO, Brewer AA (2007) Visual field maps in human cortex. *Neuron* 56:366–83.

Warnking J, Dojat M, Guerin-Dugue A, Delon-Martin C, Olympieff S, Richard N, Chehikian A, Segebarth C (2002) fMRI retinotopic mapping–step by step. *NeuroImage* 17:1665–83.

Weber B, Keller AL, Reichold J, Logothetis NK (2008) The microvascular

system of the striate and extrastriate visual cortex of the macaque. *Cereb Cortex* 18:2318–30.

Yacoub E, Duong TQ, Van De Moortele PF, Lindquist M, Adriany G, Kim SG, Ugurbil K, Hu X (2003) Spin-echo fMRI in humans using high spatial resolutions and high magnetic fields. *Magn Reson Med* 49:655–64.

Yacoub E, Harel N, Ugurbil K (2008) High-field fMRI unveils orientation columns in humans. *P Natl Acad Sci USA* 105:10607–12.

Zeki S (1990) A century of cerebral achromatopsia. *Brain* 113:1721–77.

Zeki S (1991) Cerebral akinetopsia (visual motion blindness). A review. *Brain* 114:811–24.

Zenger-Landolt B, Heeger DJ (2003) Response suppression in V1 agrees with psychophysics of surround masking. *J Neurosci* 23:6884–93.

Zihl J (2000) *Rehabilitation of visual disorders after brain injury.* Hove: Psychology Press.

Zihl J, von Cramon D (1979) Restitution of visual function in patients with cerebral blindness. *J Neurol Neurosur Ps* 42:312–22.

Zihl J, von Cramon D, Mai N (1983) Selective disturbance of movement vision after bilateral brain damage. *Brain* 106:313–40.

ISBN 978-952-60-3036-4
ISBN 978-952-60-3037-1 (PDF)
ISSN 1795-2239
ISSN 1795-4584 (PDF)